Title

THz Mixing Using Y-Ba-Cu-O Josephson Junctions Fabricated With Focused Helium Ion Beam Irradiation

Permalink

https://escholarship.org/uc/item/63s218t6

Author

Cortez, Anthony

Publication Date

2021

Peer reviewed|Thesis/dissertation

UNIVERSITY OF CALIFORNIA
RIVERSIDE

THz Mixing Using Y-Ba-Cu-O Josephson Junctions Fabricated With Focused Helium Ion Beam Irradiation

A Dissertation submitted in partial satisfaction
of the requirements for the degree of

Doctor of Philosophy

in

Mechanical Engineering

by

Anthony Cortez

June 2021

Dissertation Committee:

Dr. Shane A. Cybart, Chairperson
Dr. Luat Vuong
Dr. Peter Alexander Greaney

The Dissertation of Anthony Cortez is approved:

Committee Chairperson

University of California, Riverside

Acknowledgments

First, I would like to give thanks to God, for all things are possible through him. It was during graduate school when I began to embrace God and strengthen my personal relationship with him. I never imagined my time in graduate school would have a tremendous impact on my own spiritual faith journey. I thank God for my mind, body, and health. I pray that I may use these gifts for the purpose of fulfilling God's will. I am grateful for my advisor Professor Shane Cybart for his guidance, support, and the freedom he has given me to pursue my personal interests. Thank you for the incredible opportunities from participation in conferences to forming collaborationships with many great groups. I would also like to thank Dan Cunnane, who through his expertise in mixers played a pivotal role in this work. Thank you for serving as my mentor and sharing your office with me during my time at JPL. I also had the pleasure of spending a short time working at UCSD, my alma mater, with Bob Dynes. Thank you for this opportunity, your advice, and the many great lunch stories. To the former postdocs Ethan Cho and Hao Li, thank you for your hard work ethic and willingness to lend a helping hand or ear. To all my labmates, thank you for making graduate school so fun. Yuchao, thank you for the 5am gym sessions. Jay, thank you for the evening gym sessions when Yuchao was too tired. Stephen, thank you for reminding me to be a kid. Yan-Ting, thank you for the laughs and home-baked goods. Mom, Dad, Jr, Peter, Mini, Ricky, Vanessa, Alyssa, and Steven thank you for your unconditional love and support. To my wife, Mary, thank you for your support and willingness to critique my work. I am grateful that I was able to share my graduate school experience with you. I look forward to the many more exciting chapters and milestones in our life together.

Chapter 4, in part, has been submitted for publication of material as it may appear in *IEEE Transactions On Applied Superconductivity*, 2019, Cortez, A. T., Cho, E. Y., Li, H., Cunnane, D., Karasik, B., and Cybart, S. A., IEEE Transactions On Applied Superconductivity, 2019. The dissertation author was the primary investigator and author of this paper.

To my unborn son Noah Humberto Cortez and my late Father-in-law Dr. Humberto Schiaffino Aragon for reminding me how precious life is.

ABSTRACT OF THE DISSERTATION

THz Mixing Using Y-Ba-Cu-O Josephson Junctions Fabricated With Focused Helium Ion Beam Irradiation

by

Anthony Cortez

Doctor of Philosophy, Graduate Program in Mechanical Engineering
University of California, Riverside, June 2021
Dr. Shane A. Cybart, Chairperson

This dissertation reports the results of the investigation of a novel Y-Ba-Cu-O helium ion damaged Josephson junction mixer. Mixers, also known as a heterodyne detectors, are crucial tools for the study of spectroscopy, due to their ability to achieve the needed high spectral resolution to resolve the fine features in spectral lines. Current state of the art heterodyne detectors rely on low transition temperature superconductors, which have demanding cryogenic requirements. The motivation behind developing a high transition temperature superconducting mixer is their ability to be implemented in space and balloon missions where relaxed cryocooling is important. Commercially grown Y-Ba-Cu-O thin films are acquired and utilized for the fabrication and testing of devices. I have developed a large scale fabrication process that allows high yield throughput of patterned chips on a 2-inch wafer. In this process several $5 \times 5\,\mathrm{mm}$ devices are patterned with a planar spiral antenna, then etched to prepare for implementation of the junction at the center of the antenna. The junction is created by irradiating a focused helium ion beam on the Y-Ba-Cu-O film. These Helium Ion Josephson Junctions feature unique transport properties that are dependent upon the ion dose. For low doses of helium irradiation, the junctions have metallic barriers. For higher doses of irradiation, insulator barriers are created. The direct write process involved in the fabrication of the junction allows the junction size to be aggressively scaled down to produce high impedance devices. I have measured the DC electrical transport properties of several junctions with varying doses and widths to successfully demonstrate the ability to tune the impedance of the junction to the spiral planar antenna, which has proven difficult with other Josephson Junction mixers. The ability to match the junction impedance to the antenna improves the performance of the mixer and eliminates the need for complex circuitry that is currently used for impedance matching. The mixer performance of these devices were investigated by irradiating the junction with frequencies ranging from 90 GHz – 2.5 THz. In addition a model was developed to fit the experimental measurements and further approximate the mixer performance from existing mixer theory. I demonstrated that an existing model for Josephson junctions can be adapted to fit the experimental data for the novel type helium ion Josephson Junctions. This model is also useful for other applications outside of mixers since it can be used to determine the fundamental parameters of a junction.

Contents

List of Figures

List of Tables

Chapter 1

Introduction

1.1 Spectroscopy for Astrophysical Observations

The innate desire to explore and inhabit the unknown is a peculiar phenomena in the human species. Explorers throughout history have risked their lives for the sake of curiosity. While our ancestors sailed unruly oceans across Earth, today we sail across the vast regions of space. There exist many curiosities in our universe including the study of star formations. The life cycle of stars involves a series of steps, shown in Fig. 1.1, where each process produces key molecular identifiers in the form of a spectral line. Therefore, the recording of these spectral lines becomes the key to our understanding of studying the star formation.

In addition, spectroscopy is also useful for planetary science applications. A particular interest involves the proposed theory that the water in Earth's oceans were delivered by comets [1]. To investigate this we can utilize spectroscopy to measure and compare the

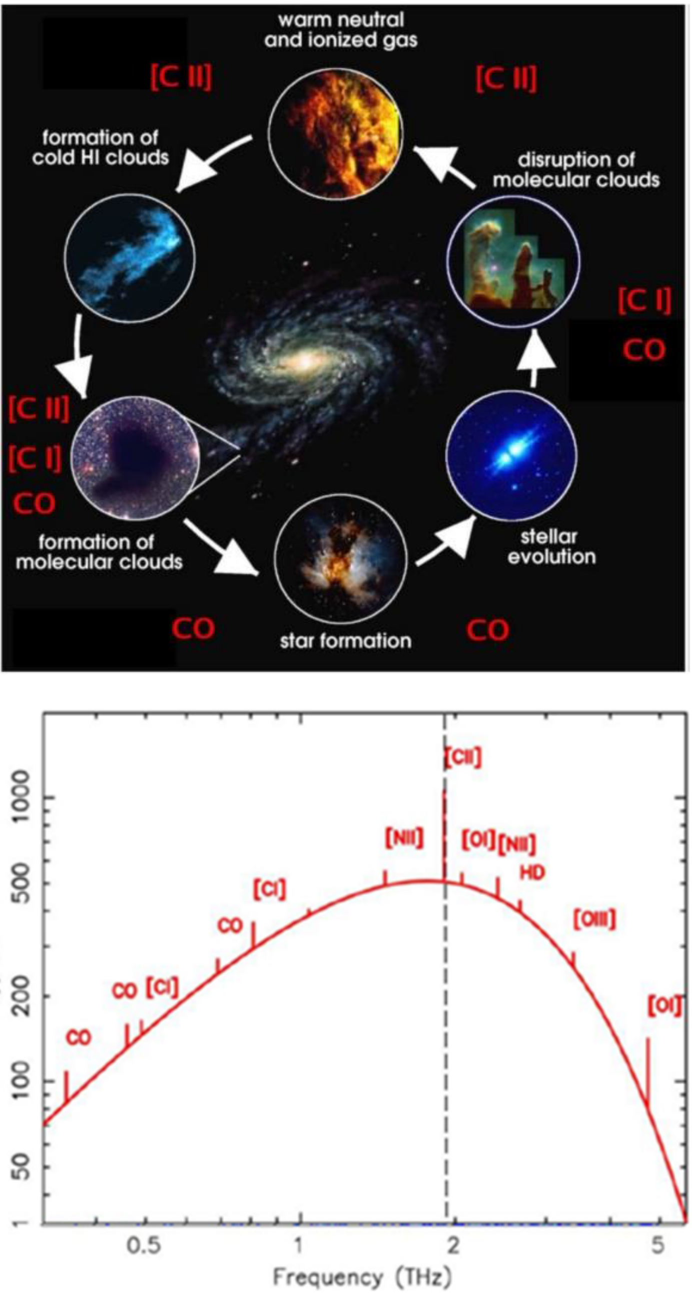

Figure 1.1: (Top) Key molecular identifiers are identified throughout each step in the life cycle of the interstellar medium. (Bottom) Spectra of some of the key molecular identifiers from the interstellar medium. A vertical dashed line is centered on the most prominent spectral line at approximately 1.9 THz.

deuterium/hydrogen (D/H) ratio of observable comets and compare it to that of Earth's [2]. Detection of these spectral lines is quite difficult in that they require high spectral resolution, $\frac{f}{\Delta f} > 10^6$, to resolve their fine features. The only detection method capable of this high spectral resolution is heterodyne detection or mixing.

1.2 Heterodyne Detectors

There is a significant technology gap in the 300 GHz to 2 +THz region either in sensitivity of the detectors or operating temperature of the detectors. In this range of the electromagnetic spectrum, high resolution detectors are needed to resolve the fine structures of the spectral lines. This is achieved through heterodyne detection or mixing of the RF signal from the sky with a local oscillator (LO) signal through a nonlinear device to produce an intermediate frequency (IF), defined as the difference between the LO signal and the RF source signal. A diagram of the mixing process is shown in Fig. 1.2. The figures of merit for mixers include: sensitivity, usually measured in noise temperature (NT), the IF bandwidth, and the LO power needed to optimally pump the mixer.

Superconductor-Insulator-Superconductor (SIS) mixers, Hot Electron Bolometers (HEB), and Schottky diodes (SD) are currently the state-of-the-art (SOA) for THz mixers. SIS mixers operate at the quantum limit (QL) up to approximately 700 GHz but losses in the ground plane superconductor cause a reduction in sensitivity above 1 THz [3]. In contrast, HEB detectors can operate at higher frequencies, but typically have NT about ten times the QL [4]. Although, it has been shown that by assuming zero optical loss and zero IF amplifier NT an HEB mixer can operate at two times the QL at 5 THz [5]. SOA NbN

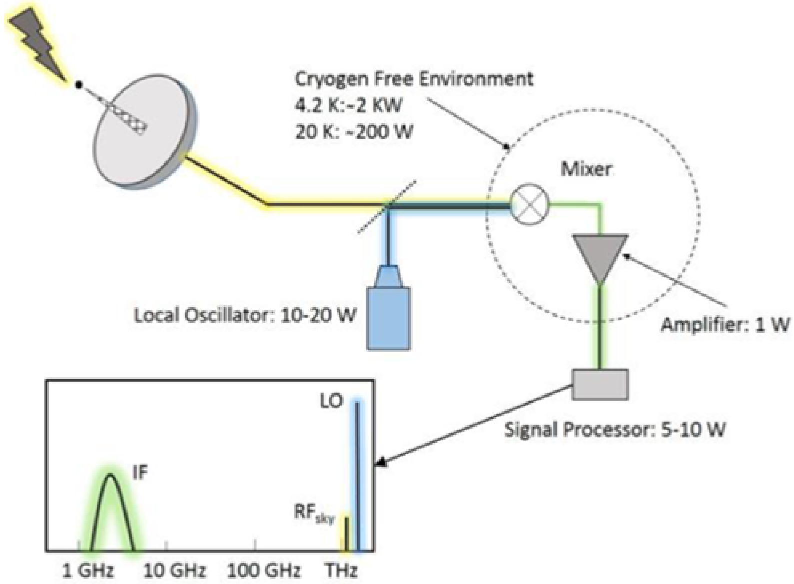

Figure 1.2: Diagram of the mixing process. The RF signal (yellow) and LO signal (blue) are fed into a mixer. The output of the mixer is the IF signal (green) which is then amplified and sent for signal processing.

HEBs have an IF bandwidth around 4 GHz [4] while more recently developed MgB_2 HEBs offer bandwidths in the 7–11 GHz range but have not yet achieved SOA sensitivity [6, 7]. SD mixers have much less sensitivity but can operate at temperatures ranging from 20 K all the way to room temperature, making them easier to develop for space instruments [8]. The major drawback to SD mixers is the large LO power requirement, on the order of $\geq$ 0.5 mW, which limits receivers to single pixel elements and restricts the upper frequency limit.

Combinations of these technologies are currently used to cover the THz spectral range which requires additional space and power. Therefore, it would be desirable to have a single mixer technology to span the full range. This thesis focuses on the research of developing a novel single mixer technology in a high temperature superconducting Josephson Mixer (HTS JM) that improves the sensitivity in the 1-2 THz region, where both SIS and

HEB experience reductions in sensitivity.

1.3 Josephson Junctions

This novel mixer will be fabricated from a superconducting material. Once the electrons in a superconductor are within 2Δ (energy gap), they will begin to pair with one another and form what are known as Cooper pairs and no single electrons can occupy a state within this energy level. The cooper pairs travel through the lattice with no scattering, therefore superconductors exhibit zero DC resistance below a critical temperature T_C.

The nonlinearity of this mixer will rely on the Josephson junction, which is a barrier separating two superconductors as shown in Fig. 1.3. Since cooper pairs are considered bosons, they can be described by a single wavefunction Ψ. The barrier can either be an insulator or a normal metal/weak superconductor. Brian Josephson derived two equations that describe the behavior of the cooper pairs tunneling through the barrier [9]. The first Josephson equation, also known as the DC relation, tells us that current can flow through the barrier with no voltage up to some critical I_C expressed as

$$I = I_C Sin(\phi). \tag{1.1}$$

Where ϕ is the phase difference between the two superconducting materials. The second Josephson equation, also known as the AC relation, gives us a relation between the time dependent phase difference and the voltage expressed as

$$V = \frac{\hbar}{2e}\frac{d\phi}{dt}. \tag{1.2}$$

The AC relation tells us that the electron pairs will oscillate proportional to the DC voltage

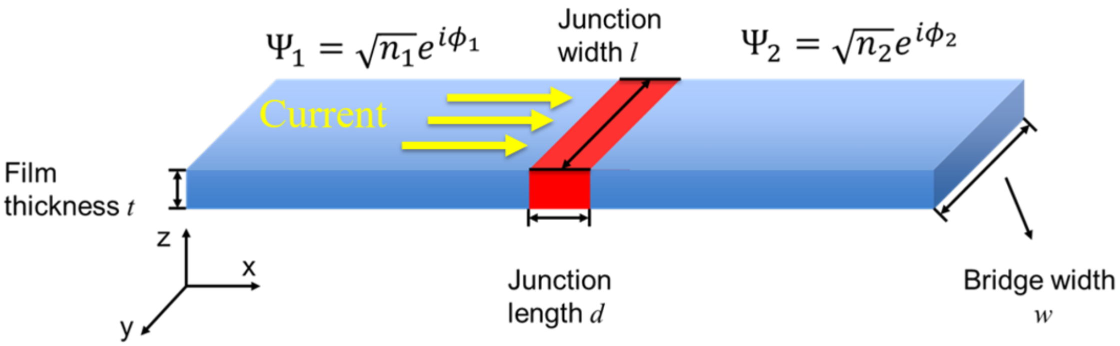

Figure 1.3: Illustration of a Josephson junction. A superconductor (blue) is separated by a thin barrier (red). Each side of the superconductor is described by a wavefunction Ψ in terms of the phase ϕ. The current (yellow) can flow from one side of the barrier to the other.

and more specifically that the maximum frequency is proportional to the energy gap ($f_{\max} \propto K_{\mathrm{J}} \cdot \Delta$) where K_{J} is the Josephson constant of 483.6 GHz/mV.

In 1968, an equivalent circuit was modeled by Stewart and McCumber that describes the Josephson Junction behavior [10, 11]. The circuit involves a resistively and capacitively shunted junction (RCSJ), where a Josephson junction is connected in parallel with a resistor and a capacitor as shown in Fig. 1.4. R_{N} is the normal state resistance of the junction (the resistance at a high voltage bias) and C is the capacitance of the junction. The current across the junction can be expressed as the sum of the currents through each component of the circuit and is given as

$$I = I_C Sin(\phi) + \frac{V}{R_N} + C\frac{dV}{dt}. \tag{1.3}$$

We can substitute in Eq. 1.2 for the voltage in Eq. 1.3 and obtain

$$I = I_C Sin(\phi) + \frac{\hbar}{2eR_N}\frac{d\phi}{dt} + C\frac{\hbar}{2e}\frac{d^2\phi}{dt^2}. \tag{1.4}$$

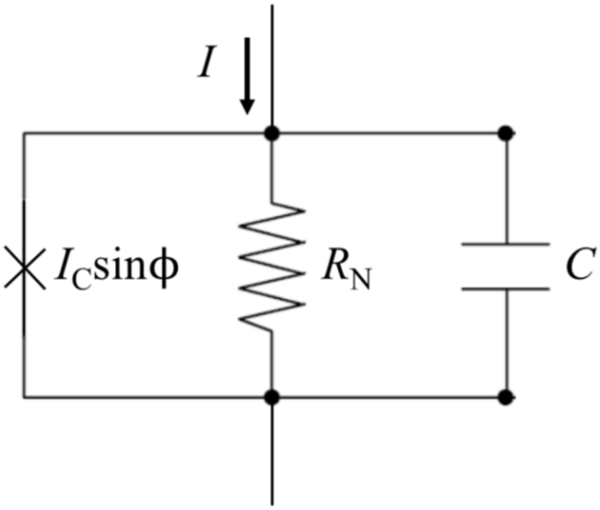

Figure 1.4: Circuit diagram of the resistively and capacitively shunted junction model. The Josephson junction is connected in parallel with a capacitor (C) and resistor (R_N).

This can be expressed in dimensionless units by dividing through I_C to give

$$i = Sin\,(\phi) + \frac{d\phi}{d\tau} + \beta_C \frac{d^2\phi}{d\tau^2}, \tag{1.5}$$

where $i = \frac{I}{I_C}$ is normalized current, $\tau = \frac{2e}{\hbar} I_C R t$ is normalized time, and $\beta_C = \frac{2e}{\hbar} I_C R^2 C$ is the Stewart-McCumber parameter. Solving Eq. 1.5 numerically for varying values of β_C will result in the current-voltage characteristics (I-V) shown in Fig. 1.5. For high values of β_C we observe hysteresis in the I-V curve, but the curve will become non-hysteretic for small values of β_c, typically less than 0.8. If the capacitance of the junction is small enough to neglect, then we can turn our second order differential equation into a first order differential equation which then has an analytical solution of the form

$$V = \begin{cases} 0, & I < I_C \\ I_C R_N \sqrt{\left(\frac{I}{I_C}\right)^2 - 1}, & I > I_C. \end{cases} \tag{1.6}$$

We can then plot this result and get the I-V characteristic curve shown in Fig. 1.6. From

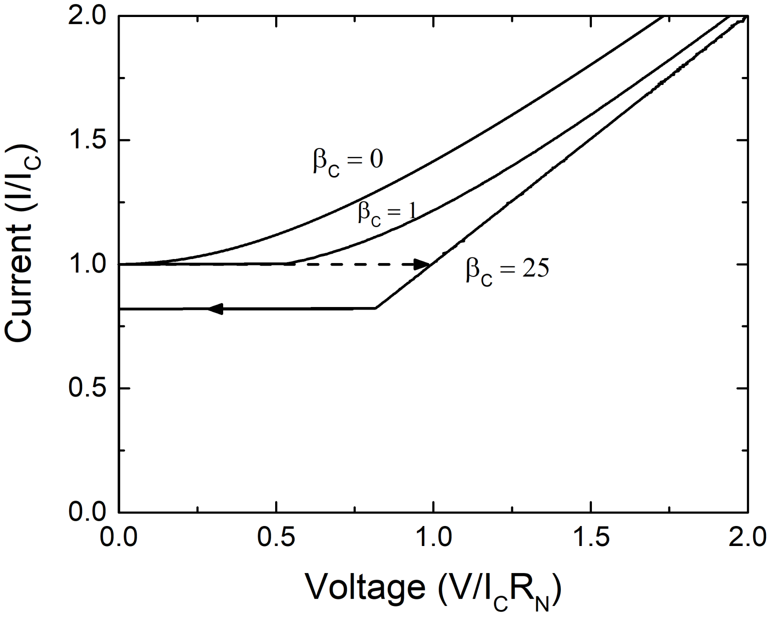

Figure 1.5: Current Voltage (I-V) characteristics of the Josephson junction solving Eq. 1.5 for varying values of β_C. Hysteresis in the I-V becomes apparent as β_C increases. The path is described by the arrows.

the I-V curve we can determine the critical voltage ($I_C R_N$), a figure of merit that describes the quality of the Josephson junction.

When the junction is driven by an AC and DC voltage source, steps will occur in the I-V curve as seen in Fig. 1.7. We can quickly derive this by starting with the first and second Josephson equations. We can substitute Eq. 1.2 into Eq. 1.1 and obtain the expression

$$I(t) = I_C Sin\left[\int \frac{2eV(t')}{\hbar} dt' + \phi_0\right]. \tag{1.7}$$

We can then assume a DC and AC voltage source taking the form

$$V(t) = V_0 + V_{AC} Cos\left(\omega_{AC} t\right). \tag{1.8}$$

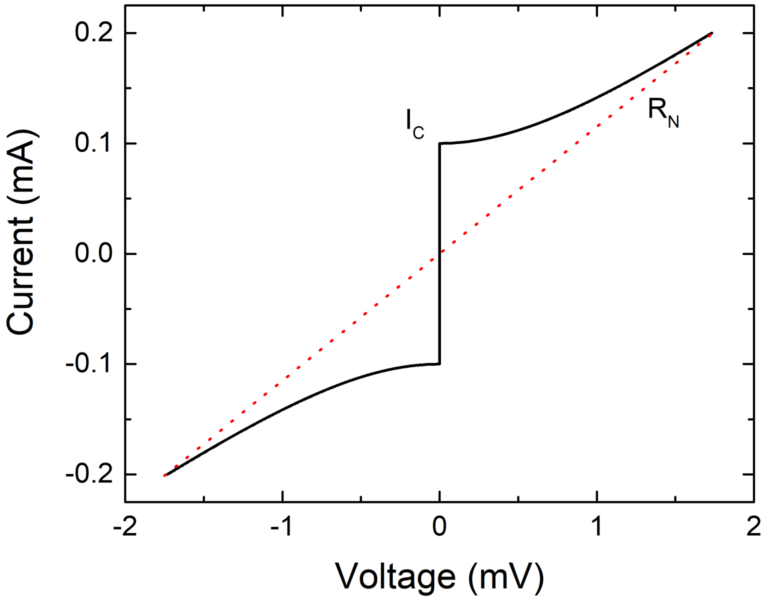

Figure 1.6: Current voltage characteristics (I-V) from solving Eq. 1.6 with $I_C = 0.1\,\mathrm{mA}$ and $R_N = 9\ \Omega$. The red dotted line intersects the origin and extends towards the normal resistance state of the curve.

Substituting Eq. 1.8 into Eq. 1.7 and utilizing trigonometric identities to integrate, we obtain the expression for current as

$$I(t) = I_C \sum_{n=-\infty}^{+\infty} (-1)^n J_n \left(\frac{2eV_{AC}}{\hbar \omega_{AC}} \right) Sin \left[(\omega - n\omega_{AC})\, t + \phi_0 \right], \tag{1.9}$$

where J_n is the Bessel function of the first kind and $\omega = \frac{2eV}{\hbar}$ is the Josephson oscillation frequency. The height of the steps depends on the amplitude of the AC source V_{AC}. These steps were first observed by Shapiro; hence the phenomenon is known as Shapiro steps [12]. The voltage steps occur in resonance described by

$$V = n \frac{h\nu}{2e}, \tag{1.10}$$

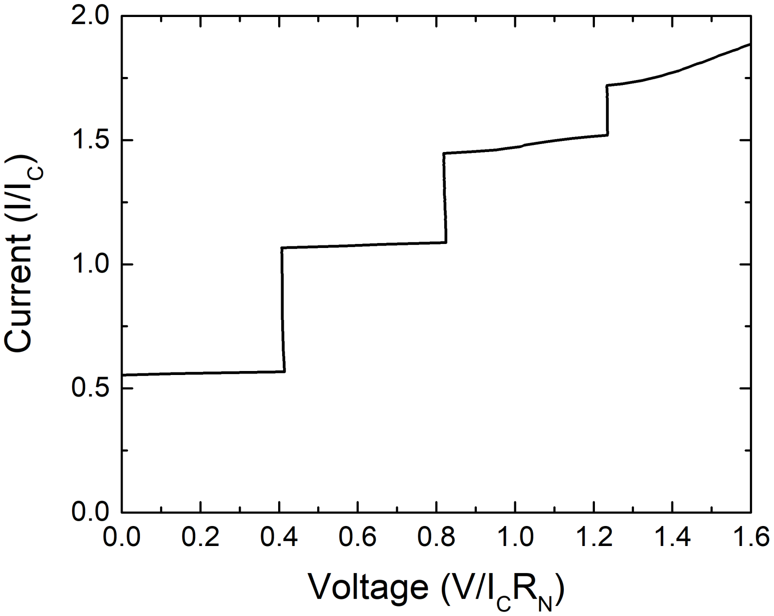

Figure 1.7: Current Voltage (I-V) characteristics of a Josephson junction irradiated with 200 GHz. The current and voltage axis are normalized and we see distinct voltage steps that occur according to Eq. 1.10.

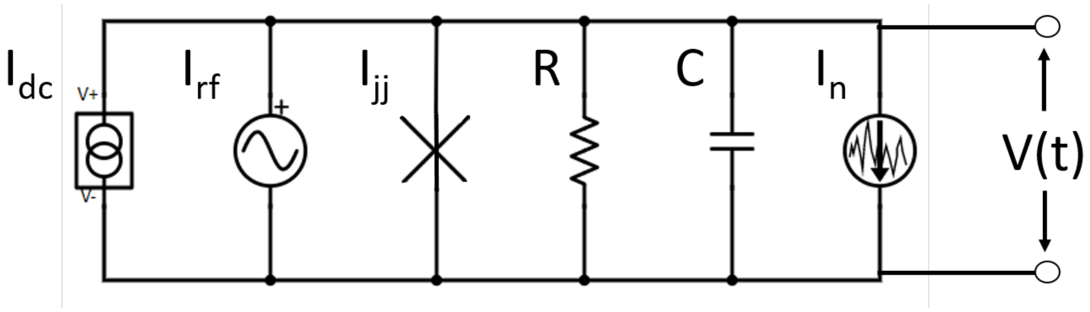

Figure 1.8: The current source circuit model utilized to solve for the current-voltage characteristics of the junctions. The Josephson junction (JJ) is shunted with a resistor (R) and a capacitor (C). I_{dc} is the DC current source, I_{rf} is the AC current source, and I_{n} is the noise current source.

where n is an integer, ν is the AC drive frequency, and h is Planck's constant.

Alternatively, we can model the AC Josephson effect by using a current source approach for the AC and DC inputs as shown in Fig. 1.8. The DC input is labeled I_{dc} and the AC input is labeled I_{rf}. I_{dc} is set by the user during the experiment as a bias current and I_{rf} is determined by the RF power irradiated at the device. We include the effects of noise as a stochastic current source, I_{n}, whose average is zero and standard deviation determined by a noise temperature [13]. We can sum the currents through the device and

Table 1.1: RCSJ Normalized Units

Description	Dimension Variable	Normalized Variable	Factor*
Current	I	i	I_{C}
Frequency	ω	Ω	$\frac{2eI_{\mathrm{C}}R}{\hbar}$
Time	t	τ	$\frac{\hbar}{2eI_{\mathrm{C}}R}$
Temperature	T	Γ	$\frac{\hbar I_{\mathrm{C}}}{2ek_{\mathrm{B}}}$

* One can return to the dimensional variables by multiplying this factor to the normalized variable.

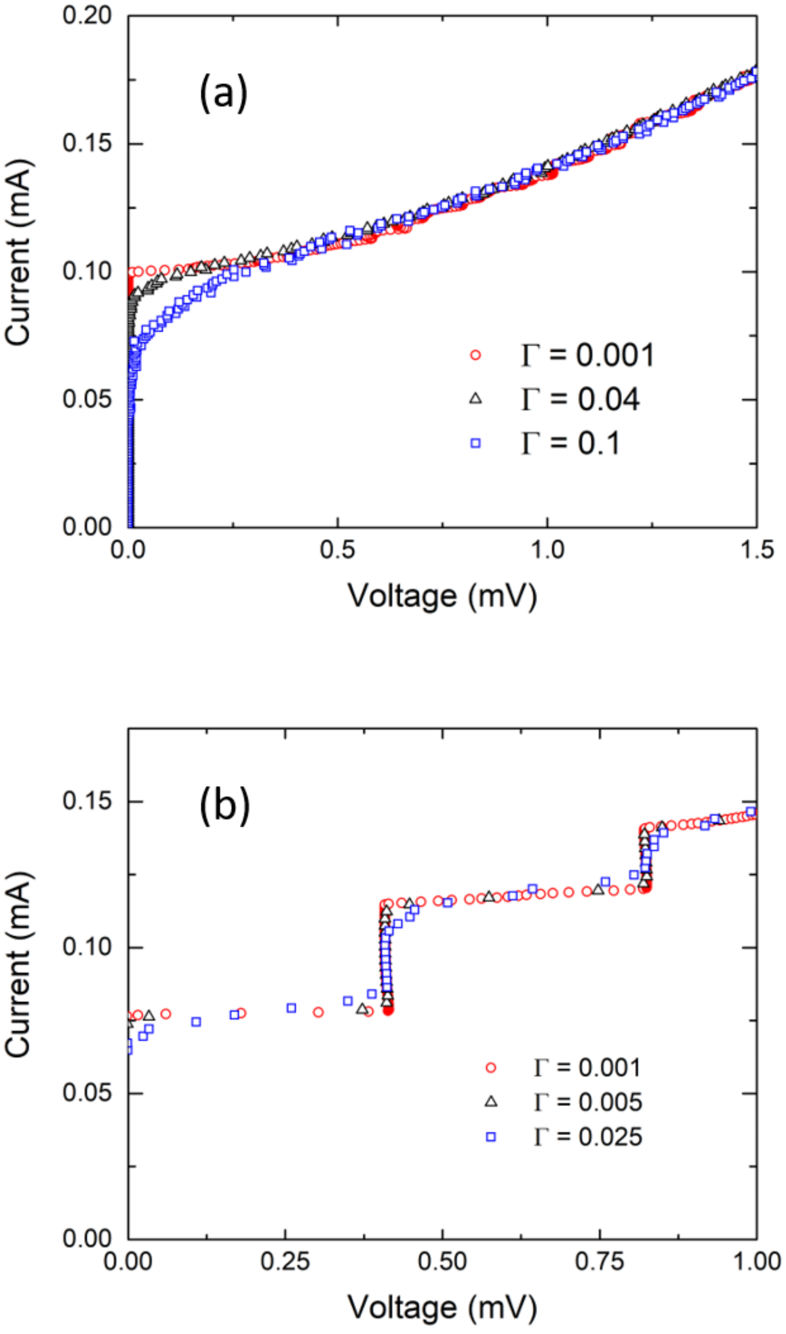

Figure 1.9: (a) Plotting non-irradiated I-V curves ($I_{\mathrm{C}} = 0.1\,\mathrm{mA}$ and $R_{\mathrm{N}} = 10\,\Omega$) for varying values of noise (Γ). As Γ increases, we see rounding of the curve near I_{C}.(b) Plotting irradiated I-V curves with the same junction parameters for varying values of Γ. Rounding is seen near each of the steps.

use the Josephson equations to write out the equation of motion for ϕ, the phase difference across the junction. Doing so gives us

$$\frac{d\phi}{dt} = \frac{2eR}{\hbar}\left[I_{\mathrm{dc}} + I_{\mathrm{rf}}\sin(\omega t) + I_{\mathrm{n}} - I_{\mathrm{C}}\sin(\phi)\right], \tag{1.11}$$

where ω is the angular drive frequency and $\hbar$ is the reduced Planck's constant. We can normalize this equation by dividing through I_{C} to give us

$$\frac{d\phi}{d\tau} = i_{\mathrm{dc}} + i_{\mathrm{rf}}\sin(\Omega\tau) + i_{\mathrm{n}} - \sin(\phi), \tag{1.12}$$

where Ω is normalized frequency and τ is normalized time. The standard deviation of the normalized noise source, σ_{n}, is given by $\sqrt{2\Gamma/\Delta\tau}$, where Γ is normalized temperature and is the ratio of the thermal energy to the Josephson binding energy. A list of the normalized constants and descriptions is shown in Table 1.1. The effects of noise on the I-V characteristics is rounding near the I_{c} as shown in Fig. 1.9(a) which plots several non-irradiated I-V curves for varying values of Γ. For no noise $\Gamma = 0$ there is no thermal rounding, but as we increase Γ we can see greater effects of the rounding in the I-V curves. The effects of thermal rounding of an irradiated I-V curve with i_{rf} held constant and Γ is varied is shown in Fig. 1.9(b). In the current source case, i_{rf} is analogous to V_{AC} in that they both determine the height of the Shapiro steps and suppression of the zero voltage current. An example of this is shown in Fig. 1.10, where we plot several I-V curves for varying values of I_{rf}. These are the nonlinearities associated with the Josephson junction that allow for the development of Josephson mixers.

The mixing process in a Josephson mixer can be better explained illustratively, through the I-V curves. First, we recall that irradiating the junction will induce steps

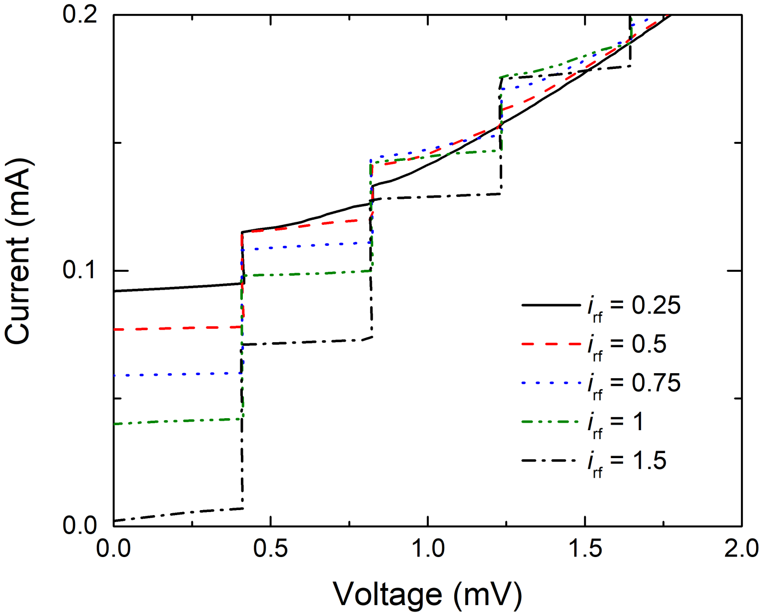

Figure 1.10: Plot of irradiated I-V curves ($I_C = 0.1\,\mathrm{mA}$, $R_N = 10\,\Omega$, $\beta_C = 0.25$, and $\Gamma = 0$) for varying values of i_{rf}. The amplitude of the steps is dependent upon the i_{rf} received.

in the curve and the zeroth step at $V = 0$ is dependent upon the pump power. This is demonstrated in Fig. 1.11, where we plot the I-V response of the junction when no irradiation is present and when it is pumped with three slightly different powers. Now let us imagine we are to begin mixing with our JJ mixer by introducing an LO signal which will result in quantized voltage steps corresponding to the LO frequency. A second signal, close to the LO frequency, is introduced to the JJ mixer which will result in a beating of the two frequencies. Therefore this is analogous to an amplitude modulation of the LO frequency at a frequency determined by the IF. The modulating LO amplitude is the equivalent of modulating the pump power and will result in a modulation of the I-V curves between the differing powers as seen in Fig. 1.11. If we were to keep a voltage-bias halfway between the zeroth and first Shapiro step during this process of modulating I-Vs we would then see a

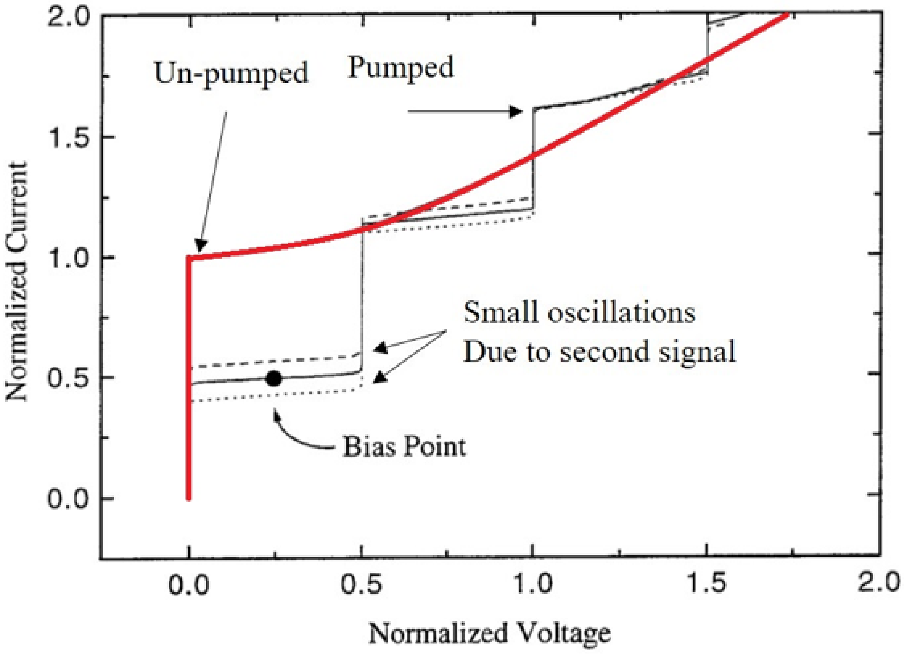

Figure 1.11: This is an illustrative method of using several I-Vs to describe the mixing process. The red curve is when the JJ is not irradiated whereas the solid, dashed, and dotted lines are I-Vs for varying pump powers. The filled circle resembles the bias point at a voltage halfway between the zeroth and first Shapiro step to better visualize the voltage swing from the small oscillations in the I-V due to the second signal [14].

large voltage swing at the IF.

1.4 Josephson Mixer History

Josephson junction (JJ) based radiation mixers have been pursued since the 1970's [15]. The only existing theory is proposed by Zmuidzinas and Schoelkopf where Nb junctions were used in the past. They claim a sensitivity limit of the Josephson mixer to be in the range of 6–20 times the physical temperature of the mixer, independent of frequency. The LO power requirements are extremely low, $< 0.2\,\mu$W, compared to existing mixer technologies. For example, at high temperature operation Schottky diode mixers require 1–3 mW. The low LO power requirements for JJ mixers is credited to the nanoscale features associated with these devices. Such low power requirements allow for the ease of constraints on heterodyne arrays utilized for space missions. Additionally, the IF bandwidth of JJ mixers are larger than those offered by other THz mixers. The large IF bandwidth of JJ mixers is credited to the fast nature of the Josephson effect. The limiting factor of the bandwidth will be determined by other receiver components, such as low noise amplifiers, rather than the mixer itself. This inherently large IF bandwidth is important at low and high frequencies. At low frequencies it could potentially be used to observe more than one spectral line without tuning the LO. At high frequencies the spectral lines become Doppler broadened and require more bandwidth to observe.

A double-side-band (DSB) NT of about 30 K, close to the theoretical prediction, has been achieved in Nb based JJ mixers below 100 GHz. However unfortunately, the NT quickly increases to 300 K as frequency increases to 500 GHz. This is likely from the presence of the intrinsic noise from Josephson oscillations and the large impedance mismatch due to the low voltage state resistance junctions [16]. It is expected that improvements can be made by addressing the issues of RF and optical loss, RF matching, and optimization of the junctions. The research presented in this thesis focuses on addressing these issues by developing a novel Josephson mixer with high T_C superconductors.

Chapter 2

High T_C Materials for Mixing

2.1 Discovery of High T_C Superconductivity

Early research on superconductivity suggested that the highest T_C would not exceed 30 K according to the Bardeen-Cooper-Schrieffer (BCS) theory [17]. Therefore, the science community was shocked when George Bednorz and Alex Müller at the IBM Zürich Research Lab discovered a ceramic superconductor to have a T_C at 35 K in 1986 [18]. A year later, 1987, researchers from the University of Alabama and Houston discovered $\mathrm{YBa_2Cu_3O_{7-\delta}}$ (YBCO) to have a T_C at 93 K [19]. This was significant because it demonstrated superconductivity existed in materials well above the boiling point of liquid nitrogen (77 K). The discovery of such a high T_C led to a frenzy in the science community and subsequently led to the discovery of several different cuprates to have a T_C above 77 K. Eagerness and excitement ensued with the many possibilities high T_C materials could offer for devices and applications such as levitating trains and supercomputers. Research in HTS electronics soared everywhere including: corporations, start-ups, government labs, and universities.

However, the advancement of HTS electronics was slow and not as simple as shifting techniques and technologies that worked for the low transition temperature superconductors (LTS) to HTS. The reason for the slow progress was because HTS have complex anisotropic properties in comparison to LTS. As a result, many of the research groups lost hope and ended their research efforts on HTS.

Fortunately, there has been a great deal of progress in the development of Josephson junctions from these complex anisotropic materials . For example, early successful JJs in YBCO were formed on bicrystal substrates. Growing YBCO on these substrates would result in a junction where the grain boundary exists. However, there was little to no control over the junction formation itself and variations in the junction properties were significant ($I_{\mathrm{C}}R_{\mathrm{N}}$ had a 30% variation). In an attempt to address the lack on control over these grain boundary JJs, researchers developed artificial grain boundary junctions. This is achieved by ion milling a ramp on the substrate and the grain boundary junction would exist at the top of the ramp. Hence, these junctions are referred to as ramp-edge junctions. This method allowed for the control in junction formation, but still had variations similar to the grain boundary junctions before. This problem of variation in junction parameters was solved with step-edge junctions. The main drawback from this technique is the complexity in fabrication due to its multilayer process. The fabrication involved a multilayer process which required multiple buffer layers for the insulating and barrier layers. Nonetheless, with the success of these advancements in HTS JJs we began to see a multitude of devices emerge, including HTS mixers [20–24]. While there exists many research efforts in pursuing HTS mixers such as YBCO HEBs [25], there are very few in HTS JJ mixers. Alternative materials and new junction fabrication techniques could hold the key to the realization of low noise Josephson mixing at higher frequencies where SIS mixers cannot operate because they are physically limited by the superconducting energy gap Δ. The maximum frequency of operation is proportional to the superconducting energy gap given by the relation $f_{\max} \propto K_J \cdot \Delta$. In addition, the energy gap of a superconductor is proportional to the critical temperature T_C. Therefore, mixers from higher T_C materials are desirable. The two main HTS materials that demonstrated satisfactory Josephson mixing are MgB_2 and YBCO.

2.2 Magnesium Diboride for Mixers

An MgB_2 Josephson mixer demonstrated successful mixing as high as 1.9 THz [26]. The junction was developed by producing weak-links in an ultra-thin film bridge of MgB_2 after ion milling. This is the most sensitive report of Josephson mixing to date. The lowest reported NT of the device was 900 K at 600 GHz and claim the potential for operation at 5 times the QL by correcting for losses in coupling. These junctions exhibited an R_N of 15–20 1 Ω. While this is higher than typical junctions (usually on the order of an ohm), these are still not the high impedance needed for optimal matching. Although the reported NT are much higher than SIS mixers, the remarkable aspect of this device was the fact that it successfully operated as high 2 THz. This is not possible for SIS mixers since they show a sharp increase in NT above 700 GHz and then rely on HEBs to cover the higher frequencies.

MgB_2 was known in the 1950's, but in 2001 it was discovered to behave as a superconductor with a bulk $T_C = 39\,K$ [27]. It has a simple hexagonal crystal structure as seen in Fig. 2.1, where the boron layers are separated by hexagonal close-packed layers

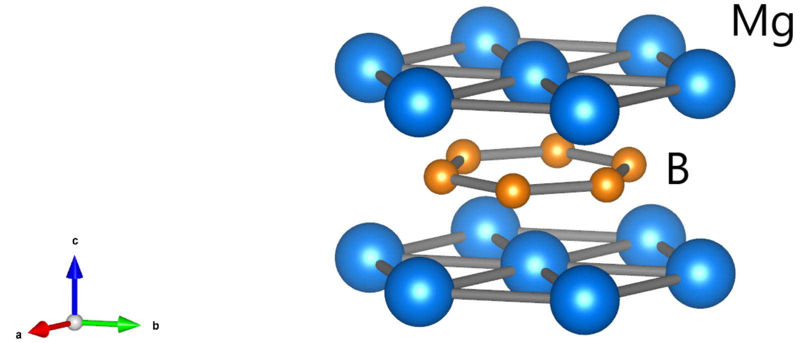

Figure 2.1: The hexagonal crystal structure of MgB_2, where Mg and B correspond to the blue and orange atoms, respectively.

of magnesium. MgB_2 is unique in that it has two superconducting gaps at 2.1 meV and 7 meV known as the π-gap and σ-gap, respectively [28–31]. Electron pairs with energies corresponding to the π-gap are free to move around in any direction of the crystal, whereas the electron pairs with energies corresponding to the σ-gap are confined to the boron planes. The superconducting coherence length is 10–20 nm, close to that of the LTS Nb. This is a surprise because the coherence length typically becomes shorter for increasing energy gaps, but this is does not seem to be the case for MgB_2. The main difficulty with MgB_2 lie within growing high quality thin films. During my first internship at NASA's Jet Propulsion Laboratory (JPL), I had the opportunity to work on a project developing a new method to grow MgB_2 for the use as HEB and Josephson mixers.

The main motivation for a new thin-film growth technology was to develop a large scale wafer process with high quality films on silicon substrates. The large scale wafer would demonstrate the ability to easily transition the fabrication process from a research and development level to a space flight mission readiness level. In addition, the ability to produce large wafers would allow for the use of deep-UV steppers for the clean sub-micron lithography features needed for mixing. The desired film qualities are high T_C ($> 35\,\mathrm{K}$), ultra-thin thick films ($< 10\,\mathrm{nm}$), and a roughness on the order of 1 nm. The high T_C will ensure higher operating temperatures especially since devices typically operate up to $0.8T_C$ to avoid too much degradation. Thin films are especially important for improving HEB performances. The IF bandwidth of an HEB is highly dependent upon the two time constants involved in the electron cooling process. These two time constants are the electron-phonon interaction time and the phonon-escape time, which is amount of time it takes for the excited phonons in the superconductor to escape into the substrate [32, 33]. It is well known that the phonon-escape time is inversely proportional to the film thickness. Not only will a thinner film improve the IF bandwidth, but it will also reduce the LO power requirements that are dependent upon the mixer volume. The roughness of the grown films will determine the device yield and spread in parameters. The ability to grow directly on Si substrates will improve high frequency transmission performance and allow for implementation of the waveguide coupled structure needed to optimally couple the LO power in arrays of HEBs [34].

The new growth technique involved modifying an atomic layer deposition (ALD) system to incorporate a thermal evaporation process that has proven success in hybrid physical-chemical vapor deposition (HPCVD) grown MgB_2 films [35]. This was achieved by simply adding a thermal evaporation source inside the ALD system as seen in Fig. 2.2. The thermal evaporation source is equipped with a custom "boat" that is suspended above the

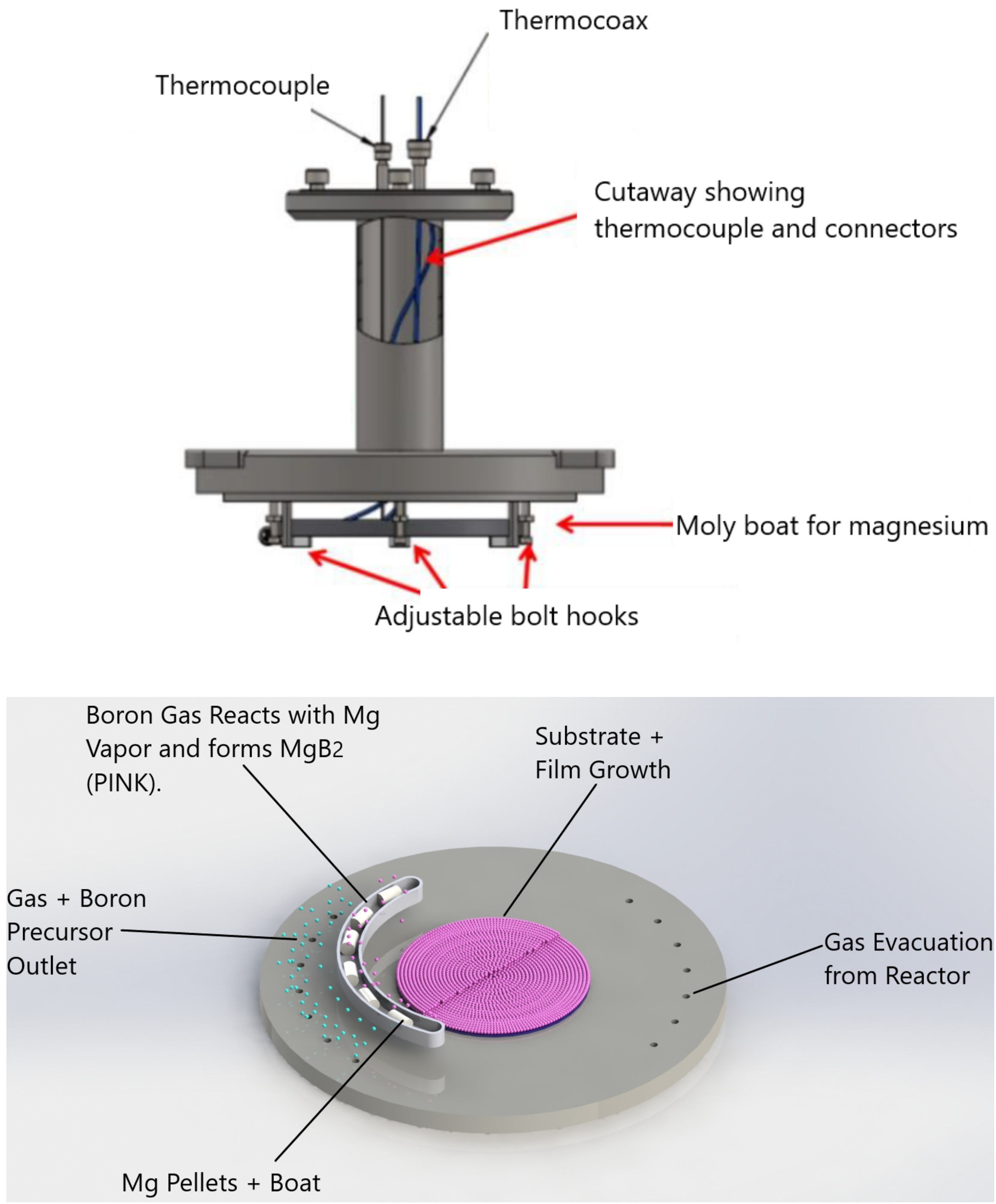

Figure 2.2: (Top) Stainless steel housing for the thermocouple and thermocoax which is connected to the suspending boat for magnesium. (Bottom) Illustration of the thermal evaporation atomic layer deposition process.

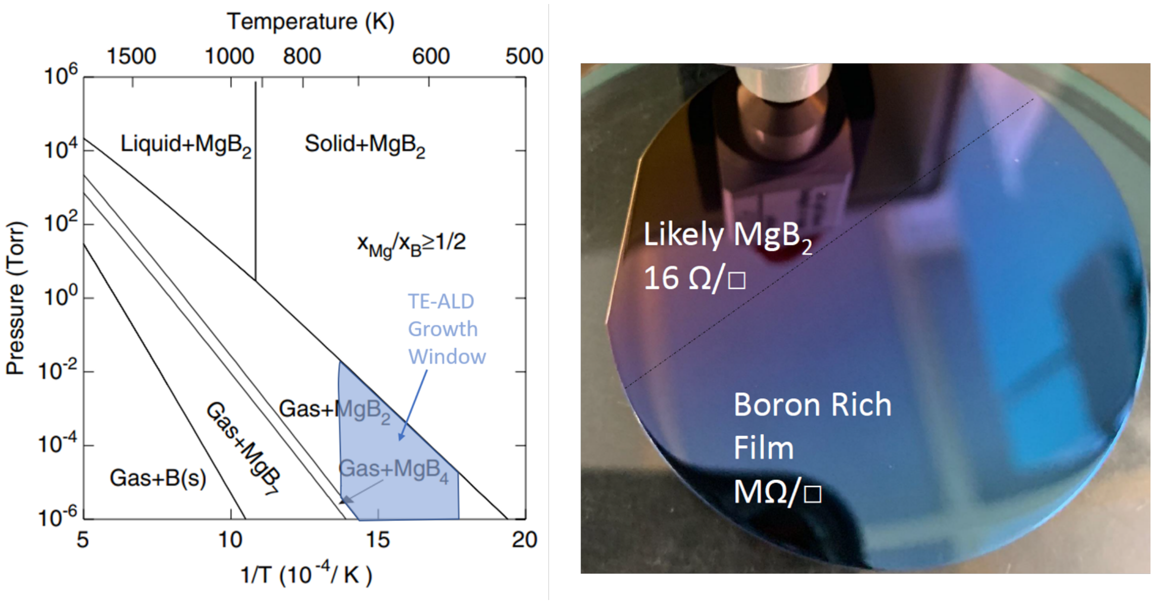

Figure 2.3: (Left) Temperature and pressure phase diagram for MgB_2 with the highlighted growth window in blue for the thermal evaporation enhanced atomic layer deposition system (TE-ALD). (Right) Result of a film growth on a 4-inch wafer. The dotted black line separates the likely boundary between the MgB_2 film to the boron rich film.

precursor outlets and the substrate surface. Mg pellets are placed in the boat and heated to provide thermal evaporation of Mg as the source. B_5H_{10} is used as the Boron source and the deposition pressure was set by modifying the H_2 flow. The gas and Boron is released from the outlet holes near the boat. The gas flows across the boat, which contains the evaporated magnesium pellets and reacts with one another. The result from the reaction is MgB_2 which then flows in a laminar fashion across the substrate surface and begins to deposit onto the substrate layer by layer. Beyond the boat and substrate are holes for the gas to evacuate. This process continues until the desired thickness of the film has been reached. The targeted growth window and the result of growing on a 4-inch wafer is shown in Fig. 2.3. We saw $16\,\Omega/\square$ immediately after deposition, but then extends to $M\Omega/\square$ along the wafer. The $16\,\Omega/\square$ is likely to be MgB_2, whereas the $M\Omega/\square$ is mostly boron. The range in resistance along the film was 16–600 Ω. One issue may be that we are oxidizing quickly in the air and thus need an *in situ* passivation step. The issue of film uniformity may be addressed by tuning the flow dynamics. This was the extent of my work with MgB_2 as my internship window was closing at JPL. While MgB_2 is attractive for device applications, the fact that there wasn't a well established vendor of high quality films resulted in shifting the remainder of my research on the material YBCO for mixing applications.

2.3 $YBa_2Cu_3O_{7-\delta}$ for Mixers

A group in Australia successfully demonstrated mixing at 600 GHz using a YBCO Josephson mixer containing step-edge JJs [36]. The reported NT was 1000 K and 2100 K at an operating temperature of 20 K and 40 K, respectively. The junctions are of high quality, but have low impedance with $R_N = 4.4\ \Omega$ leading to a significant mismatch in impedance coupling. Nonetheless, this work successfully demonstrated the ability to mix at higher operating temperatures.

YBCO is an attractive candidate to use for mixing because of its large energy gap 10–40 meV [37–40] and high transition temperature (93 K). The large energy gap correlates to a theoretical frequency limit of 4.8 THz to 19.3 THz while a high T_C will allow for the use of simple and less expensive cryocooling. In addition, YBCO is easy to process, whereas other HTS materials such as $Bi_2Sr_2CaCu_2O$ are difficult to process and are typically mechanically cleaved. However, the crystal structure of YBCO, shown in Fig. 2.4, is complex and leads to some difficulty in device fabrication. In particular, YBCO has an orthorhombic crystal structure where it is anisotropic in all directions. Not only is the crystal structure

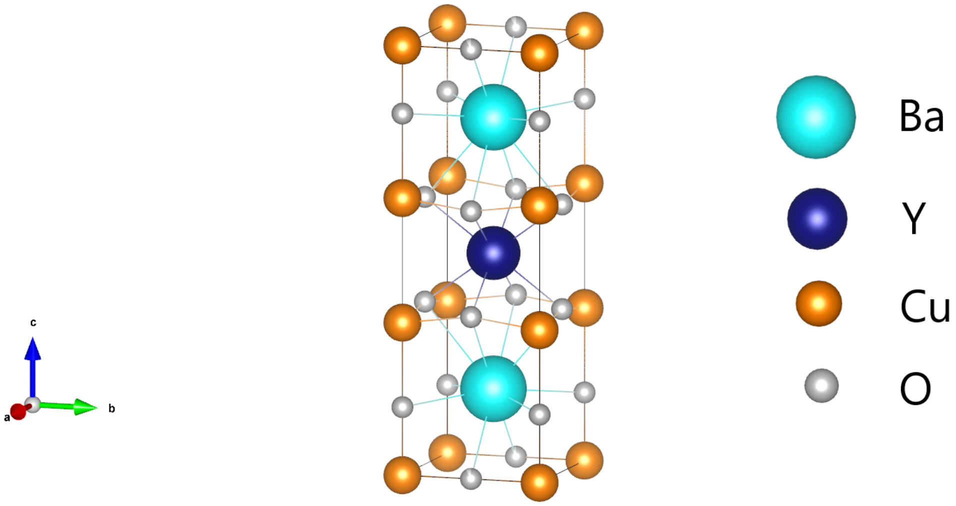

Figure 2.4: Crystal structure of YBCO reveals the anisotropy and complexity of the material structure. Electrical transport properties favor the ab-plane while high quality films are c-axis orientated.

anisotropic in all directions, but the superconducting properties are also anisotropic. The superconducting coherence length is only 2 nm in the ab-plane and an order of magnitude smaller in the c-plane with a coherence length of 0.4 nm. In addition, high-quality films are c-axis orientated and the electrical transport properties favor the ab-plane. Therefore, the multilayer techniques that have proven great success with conventional low temperature superconductors, such as niobium sandwich type Josephson junctions, are not viable for YBCO. Alternatively, a technique for developing planar Josephson junctions was required to be successful with YBCO. As discussed earlier in this chapter, some techniques that proved successful were the grain boundary, ramp-edge, and step edge junctions. The next chapter will discuss another junction technique involving ion irradiated junctions and how they can prove useful for device applications such as mixing.

Chapter 3

Ion Irradiated Josephson Junctions

3.1 Masked Ion Irradiation

The final junction technique we will discuss relies on the damage of a film via ion irradiation. A study in 1988 found that a YBCO film exhibits a metal to insulator transition when irradiated with an increasing area dose as seen in Fig. 3.1 [41]. For high doses, the material is damaged and results in the suppression of superconductivity and the material is converted to an insulator. It has been shown that junctions can be created with the use of a nano-patterned high-aspect ratio mask in combination with broad beam ion implantation. Areas of the YBCO film covered by the mask will be protected from ion damage while the uncovered areas will undergo ion damage. This technique therefore allows for control of the direction and position of the junction to be created. In addition, the junctions can be created from the starting material and eliminates the need for handling of the interfaces in other junction techniques. However, these masked implanted Josephson junctions feature low critical voltages ($I_{\mathrm{C}}R_{\mathrm{N}}$) and large excess non-Josephson currents (I_{χ}) [42] due to wide

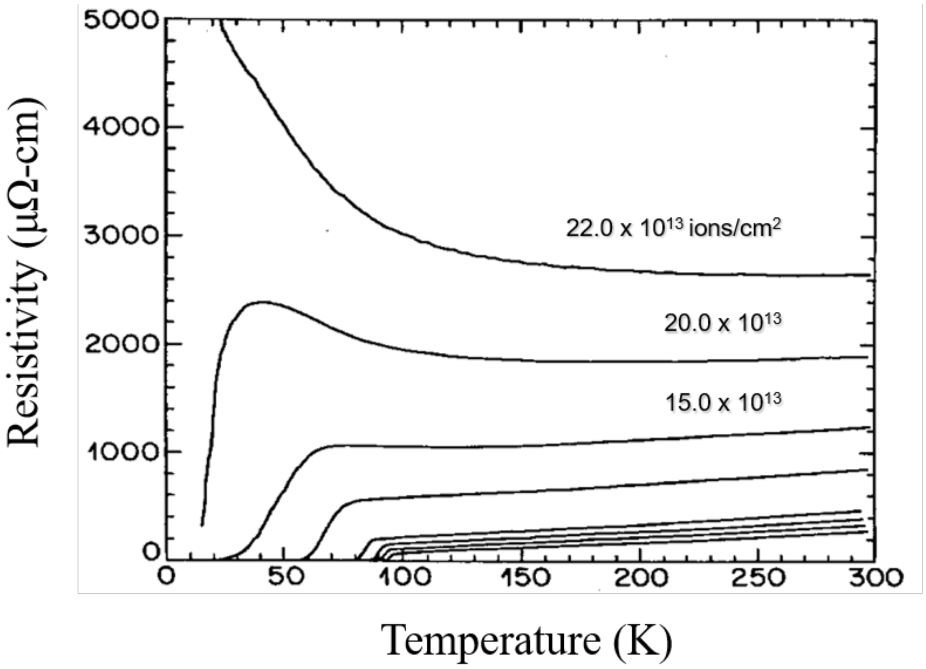

Figure 3.1: Resistivity as a function of temperature of a YBCO film for varying doses of Ne$^+$ ions. For higher doses, YBCO experiences an insulator transition [41].

and very weak diffusive Josephson "barriers" arising from device feature resolution limits, set by the particular process (typically tens of nanometers) [43,44]. To address this issue, it is necessary to have more defects in a smaller volume to produce higher quality junctions.

3.2 Focused Helium Ion Beam Junctions

With the help of advancements in technology, the issues associated with masked ion junctions can be resolved. The company Carl Zeiss has commercialized a gas field ion source that can controllably scan a 0.5 nm beam of ions. An illustration of the focused helium ion beam (FHIB) system and gas field ion source is shown in Fig. 3.2. The gas field ion source involves an emitter wire placed in an ultra high vacuum vessel (4×10^{-10} Torr) and is cryogenically cooled with liquid nitrogen. The emitter wire is applied with a

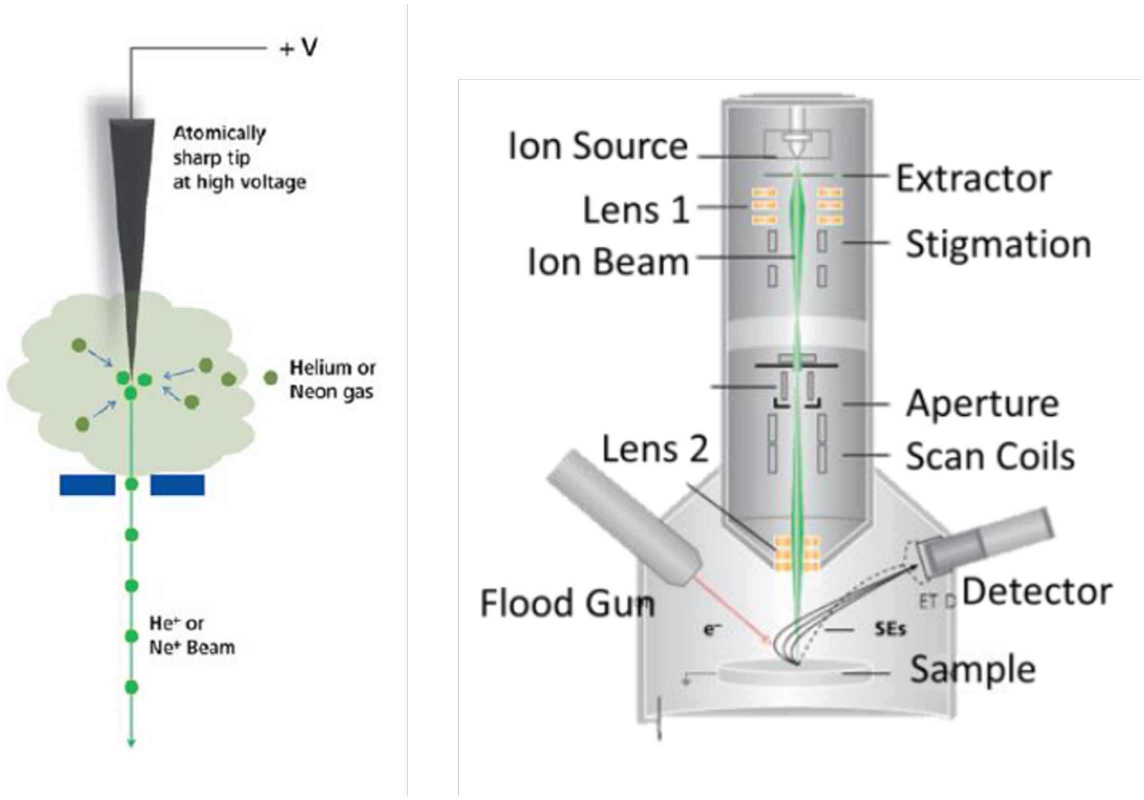

Figure 3.2: (Left) Illustration of the atomically sharp tip in the gas field with a trimer of atoms that becomes focused down to a 0.5 nm beam width. (Right) Drawing of the column of the focused ion beam system. The gas field ion source sits at the top and the ion beam travels down the column to the sample.

high voltage (30 kV) and gas is delivered into the vessel. For an atomically sharpened tip, the result is a trimer of atoms. The ion beam is sent through an extractor and down the column through a series of lenses and finally to the sample. One particular approach to device fabrication that is recently gaining traction is to utilize highly focused helium ion irradiation from a gas field ion source to create a narrow nanoscale region of crystalline defects within the material that can be utilized as a Josephson junction.

Recently, our group and others demonstrated that by confining the irradiated region to sub-10-nm dimensions with a finely FHIB that the electrical properties of ion irra-

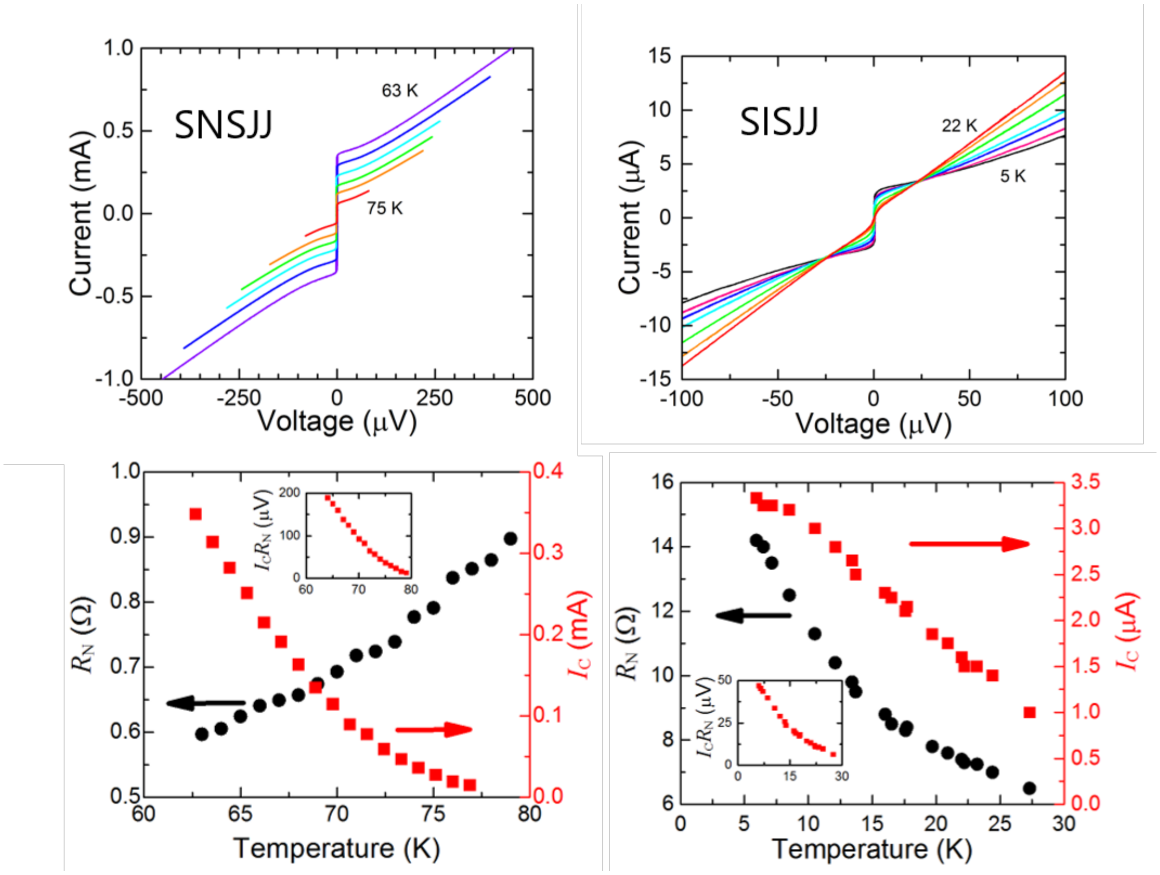

Figure 3.3: (Top-Left) I-V characteristics ranging from 63 K to 75 K for a HI-JJ irradiated with a low dose resulting in SNSJJ. (Bottom-Left) Resistance and critical current as a function of temperature for SNSJJs. (Top-Right) I-V characteristics ranging from 5 K to 22 K for a HI-JJ irradiated with a high dose resulting in SISJJ. (Bottom-Right) Resistance and critical current as a function of temperature for SISJJs. [40].

diated Josephson junctions can be affected dramatically. Specifically, Helium ion Josephson junctions (HI-JJs) were demonstrated with insulating tunnel barriers, no excess current, and very high resistance (R_N) [40, 45–47]. In addition, HI-JJs exhibit critical voltages ($I_C R_N$) approximately an order of magnitude higher than other types of irradiated Josephson junctions [48, 49], because of the much smaller critical dimension of the Josephson barrier.

At low doses, the irradiated material a normal metal and forms a barrier that behaves as a superconductor-normal metal-superconductor Josephson junctions (SNSJJ).

Whereas at higher doses the material goes through a metal-insulator-transition [46] and superconductor-insulator-superconductor Josephson junctions (SISJJ) are created. Fig. 3.3 shows the current voltage characteristics of both SISJJ and SNSJJ along with how the resistance and super current of these junctions behaves as a function of temperature. These SISJJ are markedly different from the SIS tunnel junctions used in conventional mixing. The nature of the insulator in a SISJJ is semiconducting and there are multiple transport mechanisms for conduction, eg. Mott variable range hopping, Josephson tunneling, and quasiparticle tunneling. This is in contrast to SIS junctions which typically only exhibit quasiparticle tunneling. Josephson devices from YBCO fabricated using a FHIB have exceptional potential for superconductive electronics due to the simplicity and control afforded by the single step direct-write process.

Chapter 4

Tuning HI-JJ for Optimal Impedance Matching

4.1 Impedance Matching Issues for Mixers

One of the biggest challenges with mixers is the need to match impedance within the circuit components. The development of the two-junction tuning circuit for SIS mixers was the breakthrough that led to the quantum-limited devices in that technology [50,51]. If a similar advance can be made for Josephson junctions it may bring JJ mixing to fruition. For Josephson mixers the difficulty relies on matching the impedance of the junction to that of the antenna. The relationship between the coupling efficiency of the mixer and the impedance of the various components is given by

$$E \propto 4\frac{Z_{\mathrm{A}} \cdot Z_{\mathrm{J}}}{(Z_{\mathrm{A}} + Z_{\mathrm{J}})^2}, \tag{4.1}$$

where Z_{A} and Z_{J} are the antenna and junction impedance, respectively. It is common

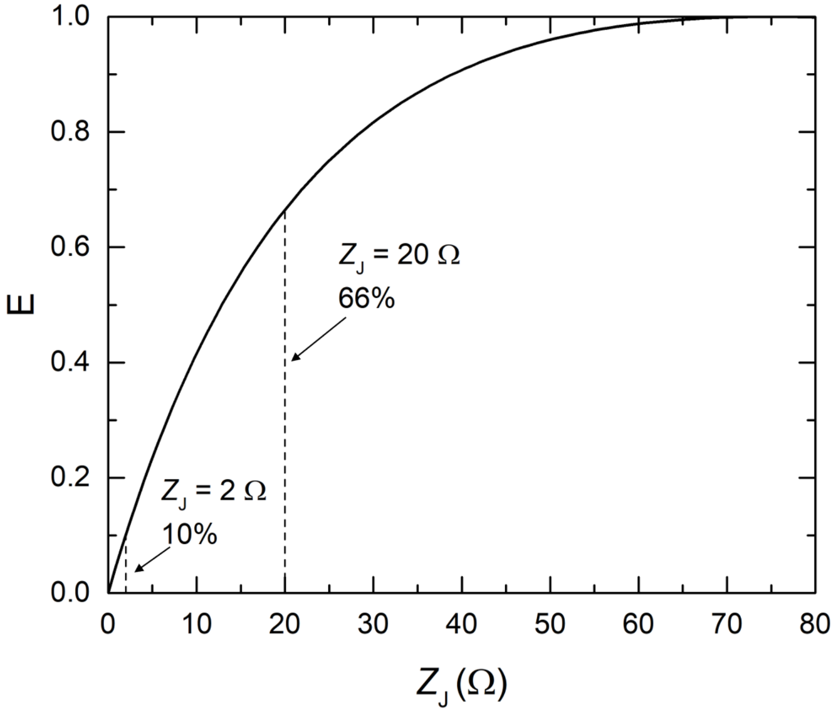

Figure 4.1: Plotting Eq. 4.1 for an antenna impedance of 75 Ω. Two vertical dashed lines are included to demonstrate the coupling percentage of a 2 Ω junction compared to 20 Ω. The coupling percentage improves quickly as we slightly increase the junction impedance.

practice to approximate the impedance of a junction to be its normal state resistance, R_{N}, while the antenna impedance is given by its geometry. For example, a logarithmic spiral antenna is known to have an impedance of approximately 75 Ω. This is difficult to match when we consider that junctions are typically on the order of just an ohm. However, the relationship given by Eq. 4.1 tells us that we can quickly improve the coupling efficiency by slightly increasing the junction's impedance as shown in Fig. 4.1. For instance, if we assume an antenna impedance of 75 Ω and a junction impedance of 2 Ω, we get a 10% coupling. However, if we were to take the junction's impedance to be slightly increased to 20 Ω, still somewhat far from the 75 Ω antenna, we get a coupling of 66%. Therefore, it is imperative to develop a method that can provide for high impedance junctions for mixing.

4.2 Fabrication of Devices

To fabricate these devices, we began with 35-nm thick YBCO thin films grown by reactive coevaporation on r-plane sapphire by Ceraco GmbH. Afterwards, a thermally evaporated 200-nm thick layer of gold was deposited *in-situ* for electrical contacts. The films were then diced into 5 mm × 5 mm chips. Large features consisting of a THz spiral antenna and contact structures were patterned into both the gold and YBCO layers using photolithography and argon ion milling. The Au must then be removed to allow the FHIB to interact with the superconducting material, otherwise the helium ions cannot penetrate through the layer of Au. A subsequent lithography step followed by a KI-I gold etch was used to uncover the YBCO bridge at the center, for irradiation of the junction. The samples were then loaded into a Zeiss Orion Plus helium ion microscope. The Josephson barrier was created by scanning the 32 kV FHIB across the center bridge which disorders oxygen in the crystal structure of YBCO, that converts the material from superconductor to insulator. The fabrication process is shown in Fig. 4.2.

A possible solution to the impedance matching of the junction to the antenna are high R_{N} YBCO nano-JJs [45, 47, 52–55]. New advances in FHIB nanopatterned YBCO junctions could yield the needed increase in performance. FHIB YBCO JJs can achieve very high resistance that could greatly benefit impedance matching. I investigated the utilization of the FHIB approach for tuning the junction impedance through optimization of the irradiation dose and the width of the junction (dimension perpendicular to the flow

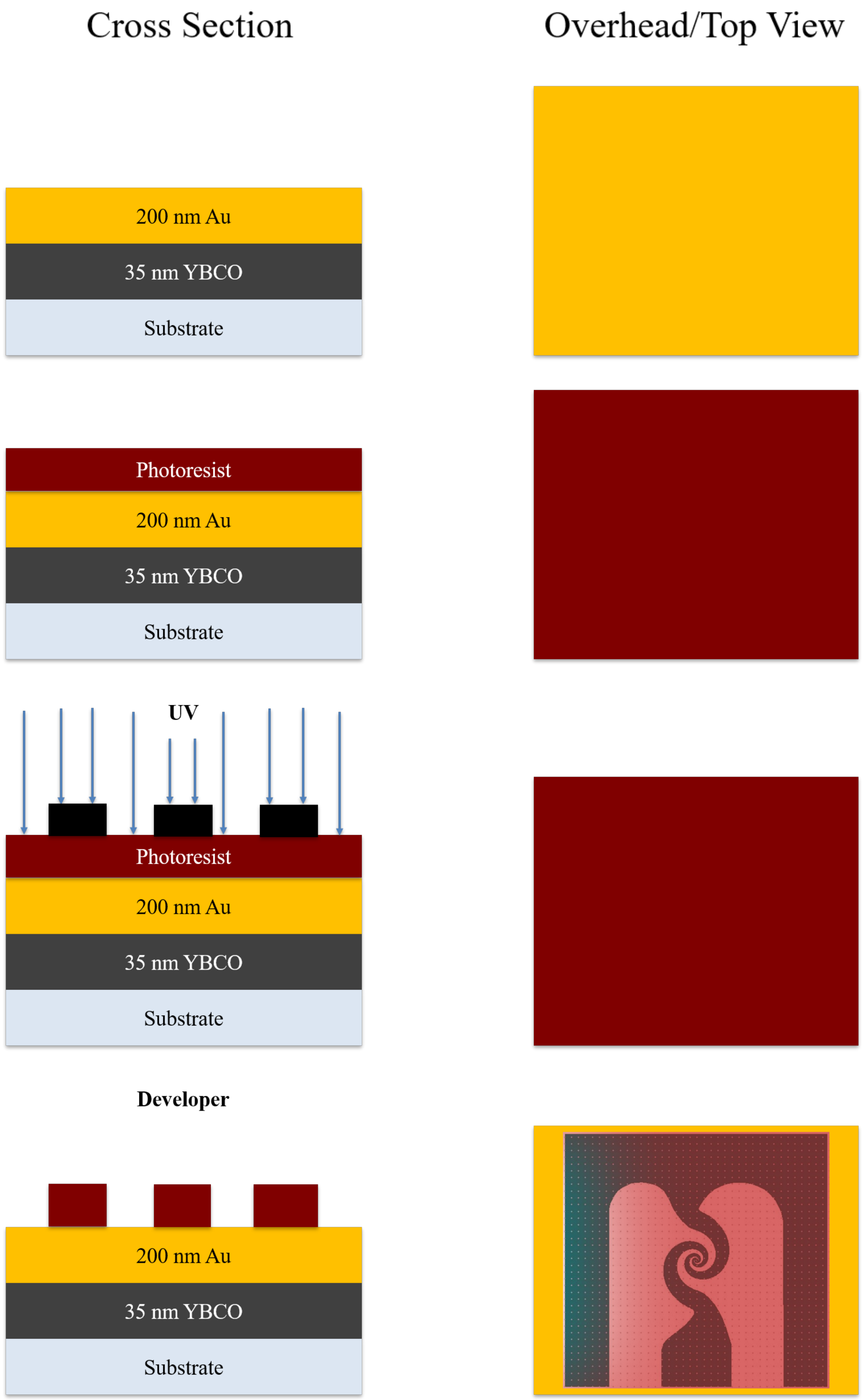
Cross Section
Overhead/Top View
200 nm Au
35 nm YBCO
Substrate
Photoresist
200 nm Au
35 nm YBCO
Substrate
UV
Photoresist
200 nm Au
35 nm YBCO
Substrate
Developer
200 nm Au
35 nm YBCO
Substrate

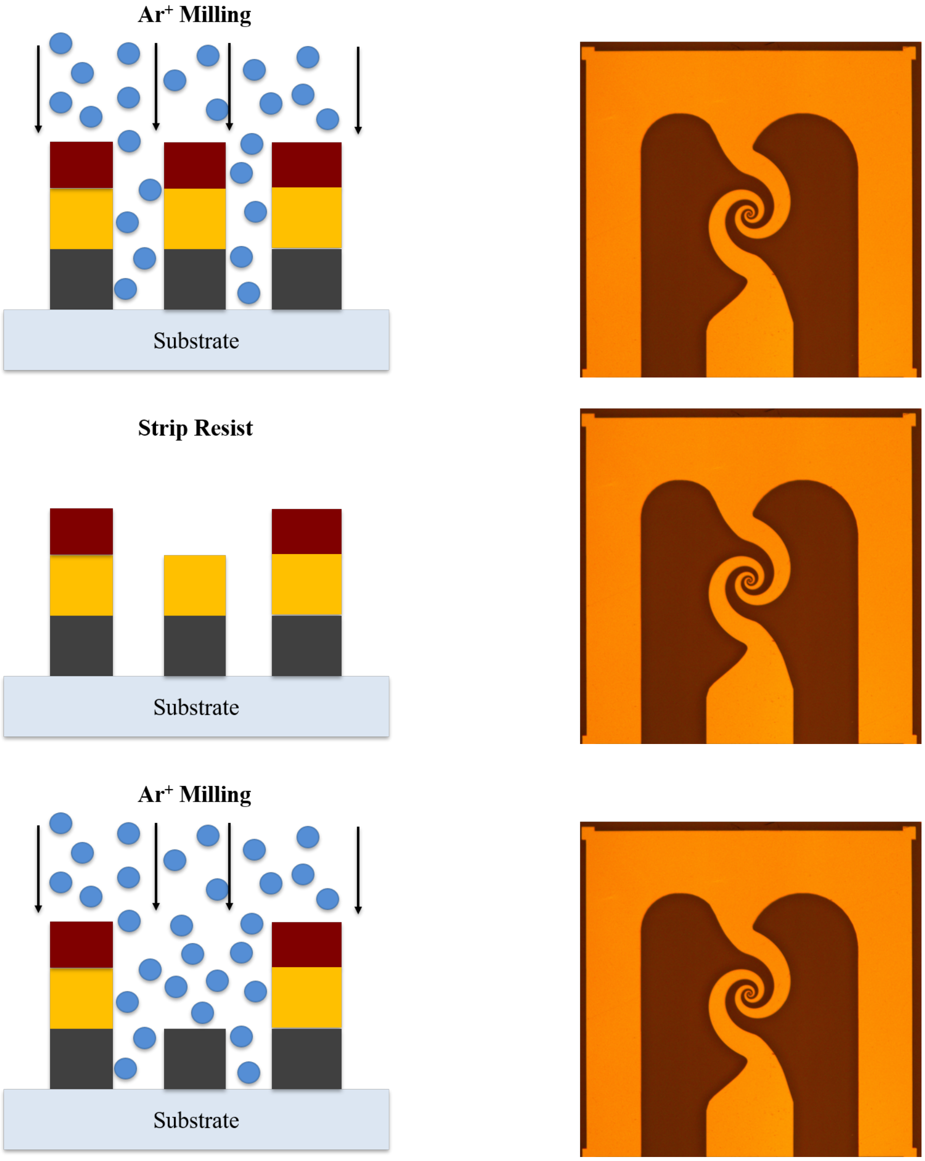

Figure 4.2: Fabrication process of devices just before the junction is created. The order of the process goes from the top down where each step consists of a cross sectional view (left column) and an overhead view (right column). We note the overhead view for the last three steps appear the same since the area involved is only 4 µm × 6 µm.

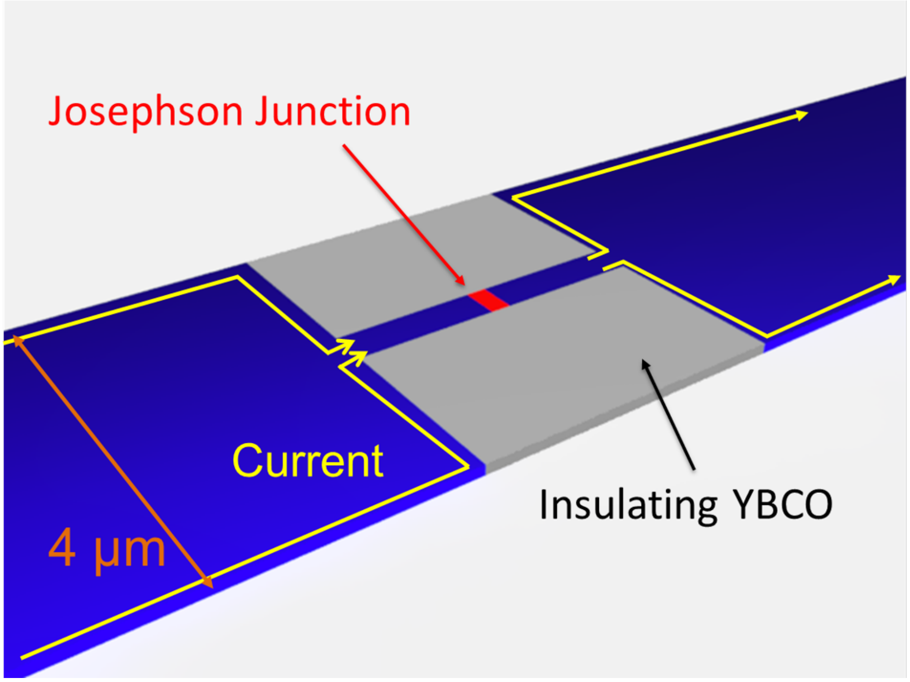

Figure 4.3: Illustration of a nano-Josephson junction fabricated with the focused helium ion beam. The blue represents a 4 µm strip of YBCO that has its edges turned insulating (grey) from irradiation of a high dose of He^+ ions. The superconducting width is effectively reduced allowing for the nano Josephson junction to be created (red). The yellow line depicts the restriction of current in the insulating areas of YBCO [45].

of current). Optimally the junction R_N should have an impedance in the range of 50–75 Ω because the impedance of a spiral antenna is known to be about 75 Ω and typical IF circuits consist of amplifiers with 50 Ω impedance. The aim is to show that YBCO junctions can be tuned to match the necessary THz and IF circuits because impedance mismatch has been a key setback for JJ mixers [56].

Common photolithography methods restrict the width of the junction to its smallest feature size to be of the order of 2 µm. However, the width of the junction can be aggressively scaled down by utilizing the FHIB. The edges of the bridge are irradiated with high doses such that the superconducting material becomes insulating, leaving only a narrow superconducting path where the junction is created. An illustration of this nano-JJ is shown in Fig. 4.3. The FHIB technique is conducive to the THz mixer application because it first, enables deep sub-um features through a trimming step with a high dose of helium ions that drives the material insulating then a JJ can be fabricated through a controlled dosage over the bridge cross section. This means that the technique gives the ability to control the junction size, as well as to tune the impedance of the junction and match the antenna.

4.3 Measurements of High Impedance Devices

In total, five spirals were created on two different chips. The first chip, M1, had a single device written with a dose of 1.2×10^{17} ions/cm^2 and width trimmed with the FHIB to 1 µm. The second chip, M2, had 4 devices with junctions trimmed to widths of 400 nm and 800 nm. In addition, on M2, the FHIB irradiation dose was varied from 1.0×10^{17} ions/cm^2 to 1.4×10^{17} ions/cm^2. We calculate the dosage from the exposure time and ion beam current measured by the in-column faraday cup. We acknowledge that this is an imprecise measurement because we see a variation in the dosage calculated in this manner after reforming the ion source. As a result, it is difficult to make accurate comparisons between junction properties and doses between different process runs.

Current voltage characteristics for several temperatures are shown in Fig. 4.4(a) for the device from chip M1. It has a maximum $I_\mathrm{C}R_\mathrm{N}$ of 800 µV with, R_N of 5 Ω. These devices are of the SNSJJ type and have diffusive normal metal barriers like those seen in masked ion damage proximity effect Josephson junctions. In proximity devices, I_C increases,

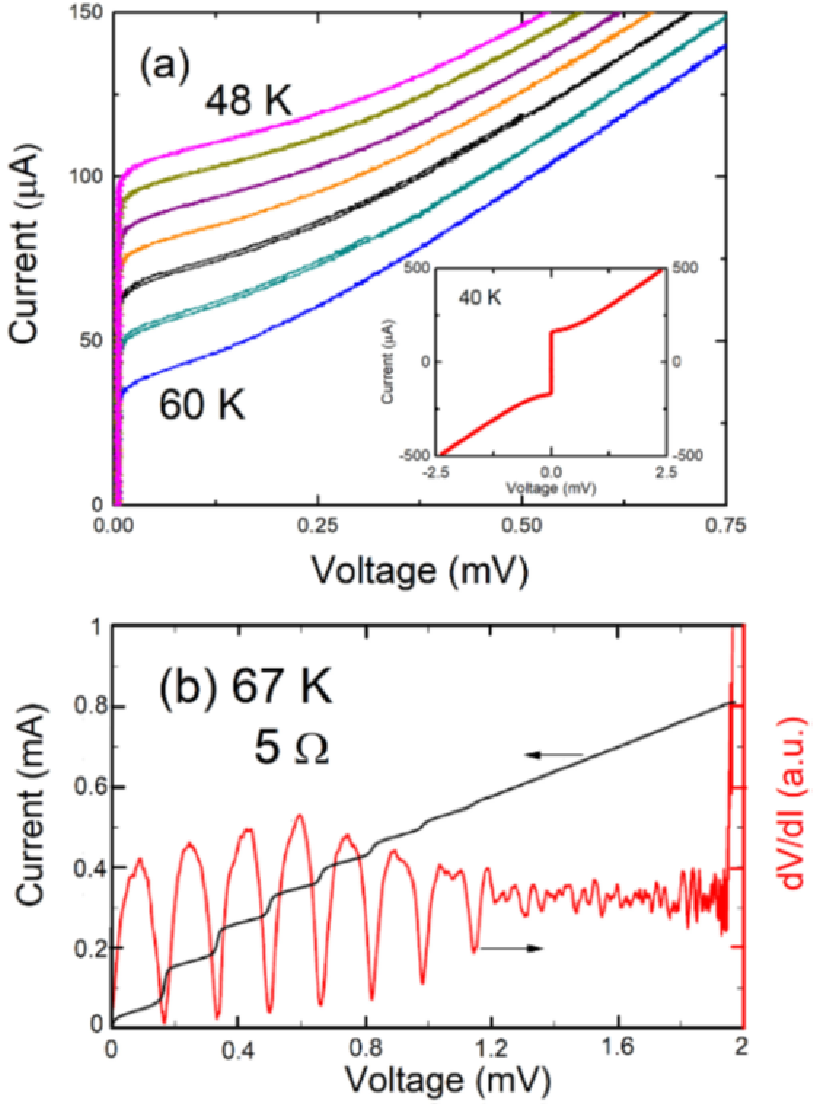

Figure 4.4: (a) *I*-*V* curve of the YBCO 1-µm-wide junction without RF irradiation taken from 48 K to 60 K in 2 K increments. An inset of the 40 K data is shown with excess current. (b) Differentiated plot of the irradiated 90 GHz *I*-*V* data corresponding to the 1-µm-wide junction, superimposed with the irradiated *I*-*V* curve taken at 67 K [57].

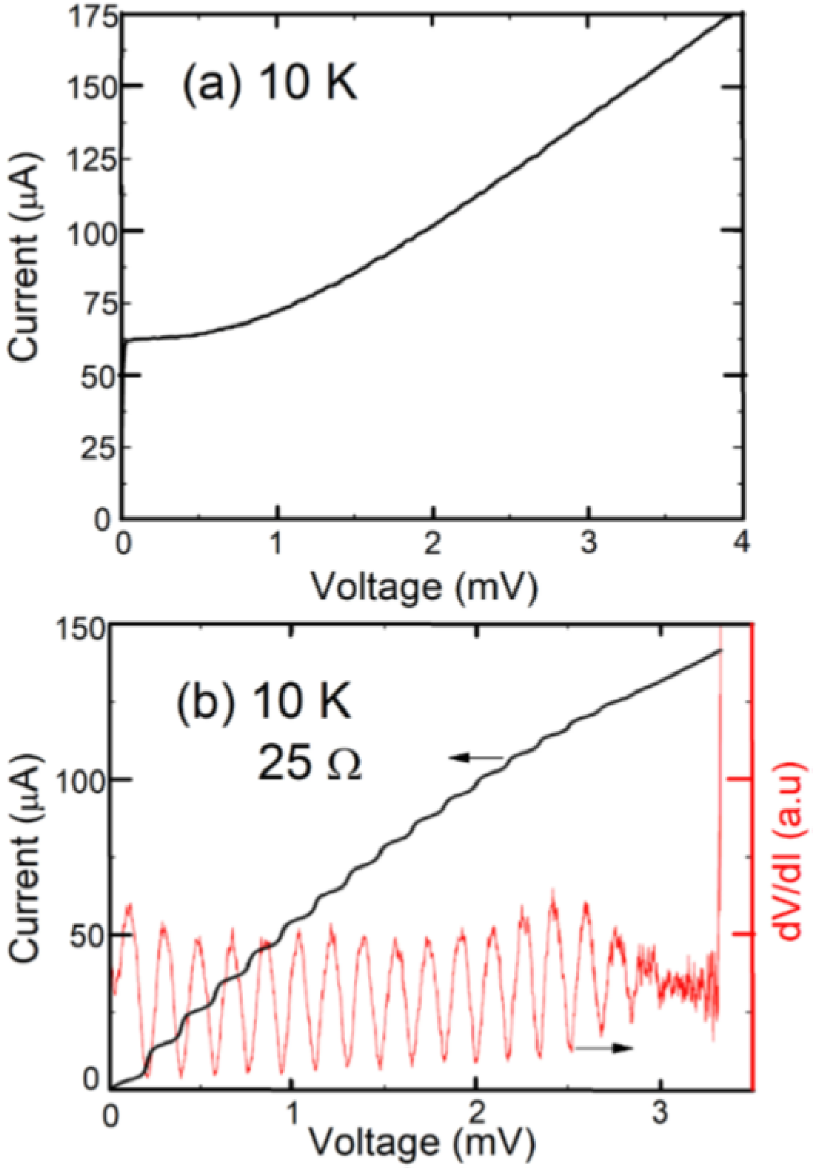

Figure 4.5: (a) I-V curve of the YBCO 800-nm-wide junction without RF irradiation taken at 10 K. (b) Differentiated plot of the irradiated 90 GHz I-V data corresponding to the 800-nm-wide junction with a dose of 1.0×10^{17} $\mathrm{He}^{+}/\mathrm{cm}^{2}$, superimposed with the irradiated I-V curve taken at 10 K [57].

and R_N decreases with decreasing temperature. At very low temperature an excess current appears at zero-voltage as seen in the inset of Fig. 4.4(a). This excess current is non-Josephson arising from Andreev reflections [58] and does not modulate in magnetic field or obey the AC Josephson relation. The AC Josephson properties of the M1 device was tested using a 90 GHz Gunn oscillator. Radiation was emitted directly into the helium Dewar without any other optics present. The pumped I-V characteristics and differential resistance for a SNSJJ are shown in Fig. 4.4(b). Shapiro steps were observed at voltages described by the AC Josephson relation given in Eq. 1.10. Steps corresponding to $n = 7$ were observed extending out to 1.2 mV corresponding to 90 GHz. For chip M2, the irradiation dosage was increased relative to that of M1 to create devices with insulating Josephson tunnel barriers. These devices had R_N that increased with decreasing temperature and no measurable non-Josephson excess current. I-V is shown at 10 K for an 800 nm wide junction in Fig. 4.5(a). R_N is approximately 25 Ω with an $I_\mathrm{C}R_\mathrm{N}$ of 1.5 mV. A consequence of decreasing the cross-sectional area of these junctions to increase R_N, is a smaller I_C and smaller Josephson binding energy, $E_\mathrm{J} = I_\mathrm{C}\hbar/\mathrm{e}$. When the thermal energy $\mathrm{k_B}T$ is of the order of E_J, fluctuations dominate that disrupt the zero voltage super current [13]. As a result, the smaller SISJJ devices must be cooled to lower temperatures to reduce thermal fluctuations. Fig. 4.5(b) shows the AC Josephson properties of the same SISJJ from Fig. 4.5(a) measured in the same experimental setup as described for the SNSJJ. Shapiro steps corresponding to $n = 17$ are observed in the pumped I-V out to 3 mV. This implies a maximum mixing frequency of 1.53 THz. Table 4.1 summarizes the properties of all the devices created for this study. M1 is shown in the first row and devices from M2 are shown in rows 2-5. As expected, we observe a trend of higher R_N with higher dose and

Table 4.1: Junction parameters used for each of the devices and their resulting R_N and $I_\mathrm{C}R_\mathrm{N}$ taken at different temperatures [57].

Dose $\left(\mathrm{He}^+/\mathrm{cm}^2\right)$	Width (nm)	R (Ω)	$I_\mathrm{C}R_\mathrm{N}$ (μV)
1.2×10^{17}	1000	5	800 (40 K)
1.0×10^{17}	800	25	1500 (10 K)
1.2×10^{17}	800	30	560 (20 K)
1.4×10^{17}	800	55	165 (15 K)
1.2×10^{17}	400	140	105 (8 K)

smaller trimmed dimension. The highest R_N of 140 Ω obtained was in the smallest junction with 400 nm width. Unfortunately, I_C was much too small for RF measurements. Table 4.1 also illustrates the lower operating temperatures of the smaller devices.

We presented the ability to effectively control R_N needed for optimal coupling to the spiral antenna and IF circuit. This was done by tuning the He ions dosage used to write the barrier and utilizing a FHIB to damage the superconductivity at the edges of the center bridge, effectively trimming the width of the junction to be created. The increase in R_N must be balanced with the accompanied decrease in I_C or the operating temperature will be suppressed by thermal fluctuations.

4.4 Shapiro Steps at High Frequencies

Devices were cooled in a helium cryostat to 7 K and *I*-*V* measurements were recorded. The HI-JJ exhibited an $I_\mathrm{C}R_\mathrm{N}$ of about 1.8 mV with a resistance R_N of 5 Ω. Irradiation was applied from a 0.6 THz source and the resulting *I*-*V* and its derivative are shown in Fig. 4.6. Shapiro steps are observed according to the AC Josephson relation, corresponding to a maximum frequency of 4.2 THz. Interestingly we observe steps well beyond the value of $I_{\mathrm{C}}R_{\mathrm{N}}$ indicating the existence of Josephson current at high voltages. A second measurement was performed on this device using a gas laser operating at 2.52 THz. The resulting I-V exhibits a $n = 1$ Shapiro step at the corresponding voltage of 5.2 mV and is shown in Fig. 4.7.

Despite the large amount of power from the laser, we still see a primary step in the I-V assuring that the HI-JJs have enough Josephson current to operate at higher frequencies where many important spectral lines exist for astrophysics and planetary science. We remark that the $n = 1$ Shapiro step height in Fig. 4.7 is far from what it would be given the non-pumped critical current. However, this is to be expected. The amplitude of the Shapiro steps is largely dependent on the normalized drive frequency $\Omega = \frac{\hbar\omega}{2eI_{\mathrm{C}}R}$, where $\omega = 2\pi\nu$. For $\Omega < 1$, the amplitude of the Shapiro step height is reduced [59]. For the other case when $\Omega > 1$, the classical penetration depth of the barrier limits the field penetration into the junction rather than the Josephson penetration depth [60] and therefore, also reduces the amplitude of the step. In order to optimize the amplitude of the steps, Ω should be near 1. The device used in Fig. 4.7 has $\Omega = 2.895$, therefore we see the expected reduction in the amplitude of the $n = 1$ step. To optimize Ω, that is to have $\Omega = 1$, we need an $I_{\mathrm{C}}R_{\mathrm{N}}$ of 5.2 mV. Although the device is not optimized to produce large Shapiro steps at 2.52 THz, it is still encouraging to see that the Josephson effect occurs at such a high bias given an $I_{\mathrm{C}}R_{\mathrm{N}}$ of 1.8 mV. These results are exciting for potential use of HI-JJ in THz applications.

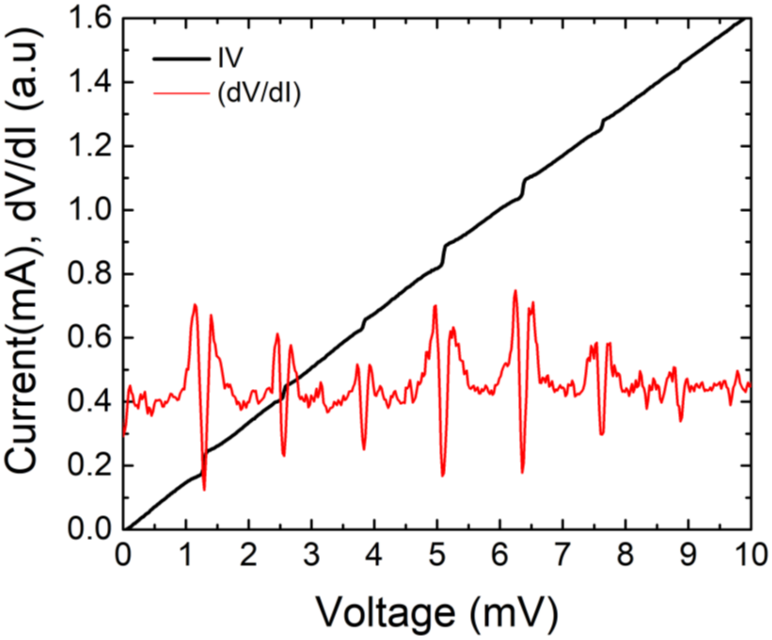

Figure 4.6: I-V plot revealing $n = 7$ Shapiro steps at integers of $1.24\,\mathrm{mV}$ from the $0.6\,\mathrm{THz}$ source. $\mathrm{d}V/\mathrm{d}I$ is also plotted.

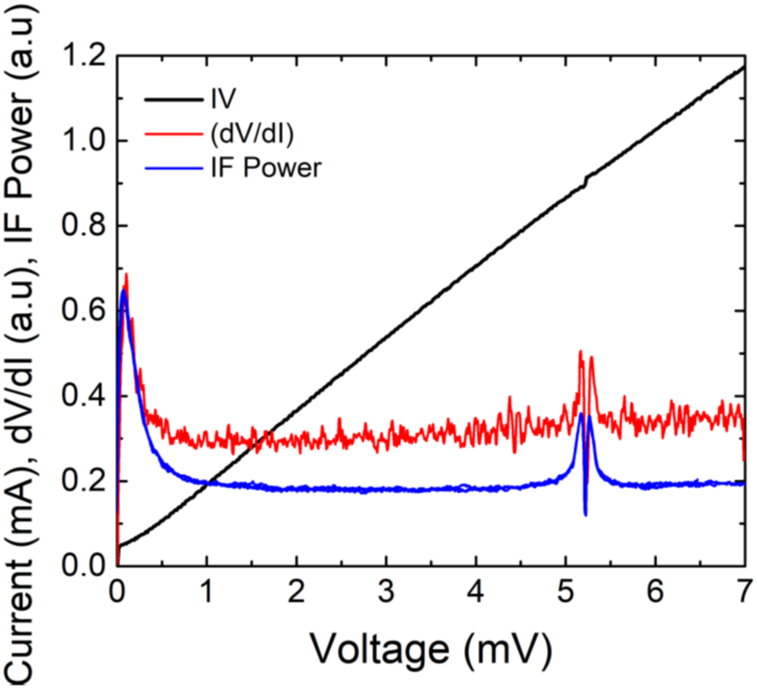

Figure 4.7: I-V plot revealing the primary Shapiro step at 5.2 mV from a 2.52 THz gas laser. $\mathrm{d}V/\mathrm{d}I$ and the intermediate frequency (IF) power are also plotted.

Chapter 5

YBCO HI-JJ Mixer Performance

5.1 Experimental Setup

A quasi-optical setup is utilized to perform the experimental mixing measurements of the HI-JJ devices. The device has its backside substrate mounted to a Si lens designed to couple free-space radiation to the junction. The mixer and lens are placed on a mixer block that sits inside a 4.2 K dewar with a Mylar optical window. A DC bias line is fed through the dewar and to the mixer block. A cryogenic low noise amplifier (LNA) and a room temperature (RT) amplifier are used in the IF circuit line. The mixer noise temperature was determined using the conventional Y-factor technique which involves comparing the IF output power under a hot and cold thermal load from a blackbody. The noise temperature is defined as

$$T_{\mathrm{N}} = \frac{T_{\mathrm{HOT}} - Y T_{\mathrm{COLD}}}{Y - 1}. \tag{5.1}$$

$Y = P_{\mathrm{HOT}}/P_{\mathrm{COLD}}$ is the Y-factor and T_{HOT} and T_{COLD} are the load temperatures used. Typical hot and cold load temperatures are 300 K and 77 K, respectively, since they are

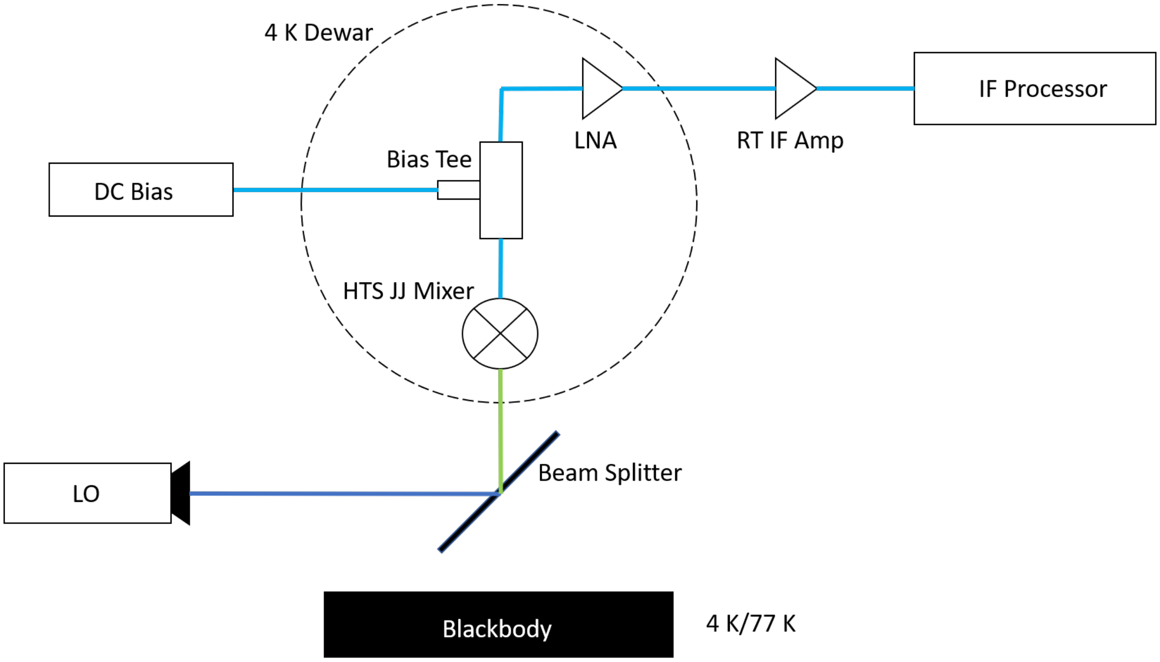

Figure 5.1: Schematic of the mixing noise temperature measurement. The mixer, bias tee, and low noise amplifier (LNA) are housed in a 4 K dewar while the LO and blackbody signal enter via a Mylar window.

easily accessible via room temperature and liquid nitrogen. A Mylar beam splitter is used to couple the LO signal with the thermal loads. A schematic of the measurement setup is shown in Fig. 5.1.

5.2 Noise Temperature

Following the fabrication technique involved in creating nano-HI-JJs, we were able to obtain a device that had its impedance well matched with the antenna and IF circuit. This device has a $R_{\mathrm{N}} = 62\ \Omega$ and $I_{\mathrm{C}} = 7\ \mu\mathrm{A}$ as shown in Fig. 5.2. A 600 GHz solid state frequency multiplier source was used as the LO and delivered to the device as described above. The conventional Y-factor method is used to determine the noise temperature of the device. While the device is pumped with 564 GHz LO, we examine the IF power output of the device as seen in Fig. 5.3. The voltage step at approximately 1.17 mV corresponds to a frequency of 564 GHz. The hot load and cold load used for this measurement were 300 K and 77 K, respectively. The minimum noise temperature of our device at 564 GHz is 980 K. Several YBCO mixers have recently been demonstrated [61–63] and the best reported Josephson mixer noise temperature to date at 600 GHz is 1000 K [36], which uses a step-edge technique for creating the junction. Fig. 5.3 plots the noise temperature (right Y-axis) of our device at different bias voltages when pumped with 564 GHz LO. We see sub-1000 K noise temperature when biased at halfway between the zero and first voltage step, a competitive value compared to the aforementioned 1000 K step-edge junction. This is a very promising result and is even more encouraging when we consider that losses of signal can still be accounted for. With optical optimization, we can expect to improve the sensitivity by a factor of 5-10. The device measured had great impedance matching to the antenna, therefore we do not expect much loss from impedance mismatch. However, the substrate used, non-polished sapphire, is not optimal for this application because the device is irradiated from the backside of the substrate. In addition, no anti-reflection coating is used which is expected to account for about 30% loss of the signal.

One concern is if this noise temperature fully corresponds to mixing or if there may be some direct detection involved at frequencies not near the LO. Direct detection is a possibility since we are using a blackbody as the load which has a broadband spectrum. This has proven to be a common problem with wide-band coupled Josephson mixers in the past. However, we are confident that there is no direct detection involved in this Y-Factor

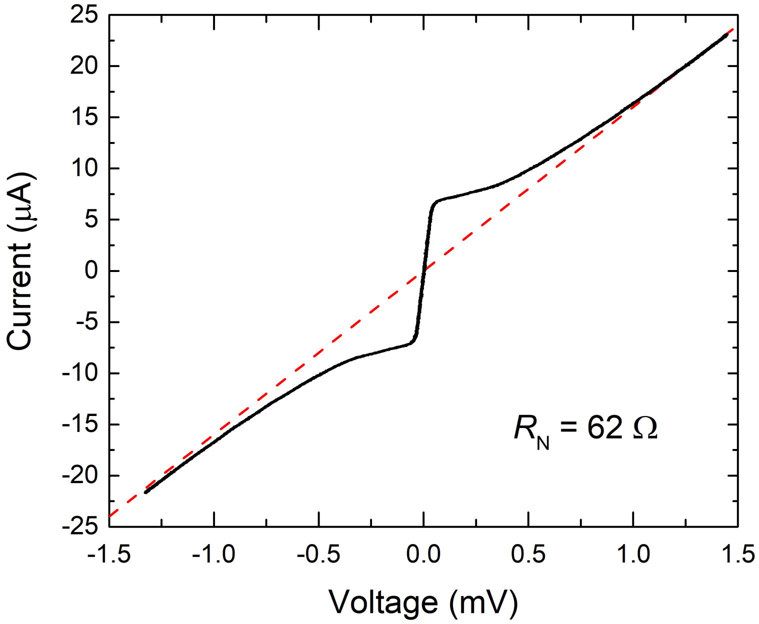

Figure 5.2: I-V characteristics of a well tuned device to match the impedance necessary for the antenna and IF circuits. The junction has a critical current of 7 µA and a resistance of 62 Ω. The red dashed line reveals no excess current present in the junction.

measurement for two reasons. One, we utilized a copper mesh filter centered near 600 GHz which rejects any radiation out of band. Two, no features of the I-V curve revealed any dependence with changes to the load temperature. It is important to note that although the impedance of the device was well matched to the antenna and IF circuit, this device exhibited low critical current. Ideally, we would like to improve the critical current of the junction on the order of hundreds of microamps where we can achieve mV $I_\mathrm{C}R_N$ products and increase the IF output power.

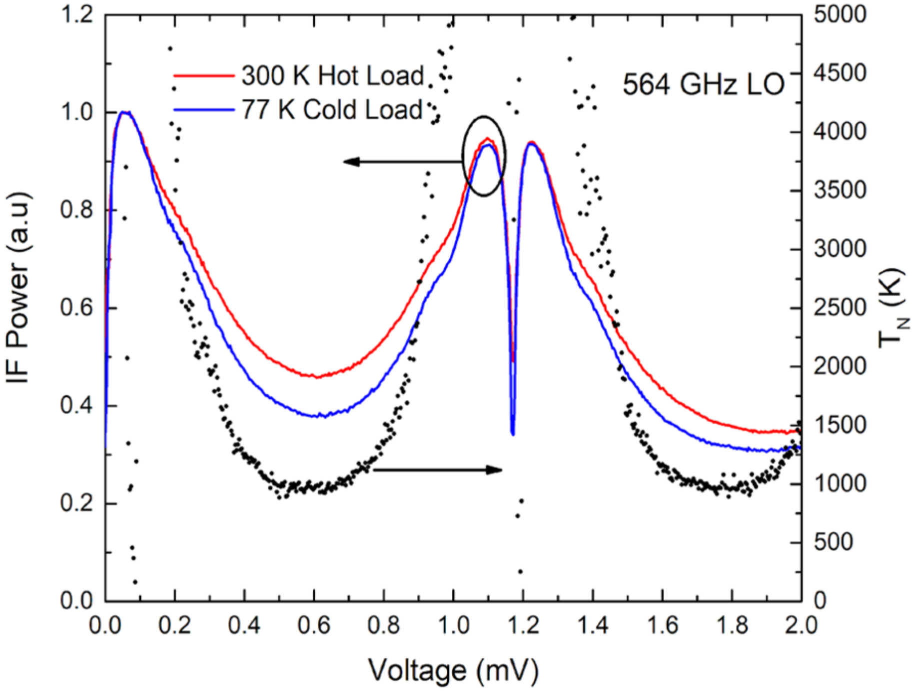

Figure 5.3: Plot of the IF output power (left y-axis) of a HI-JJ mixer with an LO of 564 GHz under a hot (red) and cold (blue) load. The noise temperature from the IF power response is plotted in black (right-axis).

5.3 Conversion Gain

The conversion efficiency, a key parameter for mixer performance, can be determined through analysis of the frequency-conversion matrices as described by Tuar [64]. In this method, the mixer can be described as a linear network with various ports corresponding to different frequencies. We follow the three port model which consists of the intermediate frequency (f_{IF}), upper side-band frequency ($f_{USB} = f_{LO} + f_{IF}$) and the lower side-band frequency ($f_{LSB} = f_{LO} - f_{IF}$). The linear relationship between the small signal voltages and the small signal currents involved at these three frequencies can then be expressed as:

$$\begin{pmatrix} V_{USB} \\ V_{IF} \\ V^*_{LO} \end{pmatrix} = \begin{pmatrix} Z_{UU} & Z_{UO} & Z_{UL} \\ Z_{OU} & Z_{OO} & Z_{OL} \\ Z_{LU} & Z_{LO} & Z_{LL} \end{pmatrix} \begin{pmatrix} I_{USB} \\ I_{IF} \\ I^*_{LO} \end{pmatrix}, \tag{5.2}$$

where $\tilde{Z}$ is the impedance matrix. The impedance matrix elements are determined by solving the nonlinear pumped case of the mixing element to obtain functions of the DC and LO voltages with respect to varying LO powers [64–66]. In this case, our nonlinear mixing element is a Josephson junction, which consists of a thin barrier separating two superconductors and can be described by Josephson's two equations [9]

$$\begin{aligned} I &= I_C \sin\phi \\ V &= \frac{\hbar}{2e}\frac{d\phi}{dt}, \end{aligned} \tag{5.3}$$

where I_C is known as the critical current of the junction and ϕ is the difference in the phase of the two superconducting regions. The first equation tells us that current can flow from one superconducting region through the barrier to the other superconducting region with zero voltage up to some critical current, I_C. The second equation tells us that the DC voltage across the junction is dependent upon the change in superconducting phase difference over time. It has been shown that JJs can be described using the resistively and capacitively shunted junction (RCSJ) model [10, 11]. With this model the equivalent circuit consists of a resistor and capacitor in parallel with the Josephson element itself and is shown in Fig. 1.8. We include the effects of thermal fluctuations by introducing a stochastic current source. With a DC and LO current source we can sum the currents through the device and use the Josephson equations listed in Eq. 5.3 to write out the equation of motion for, ϕ, the phase difference across the junction. Doing so gives us

$$\frac{C\hbar}{2e}\frac{d^2\phi}{dt^2}+\frac{\hbar}{2eR}\frac{d\phi}{dt}+I_C\sin\left(\phi\right)=I_{DC}+I_{LO}\sin\left(2\pi f_{LO}t\right)+\delta I_N\left(t\right), \tag{5.4}$$

where C and R are the capacitance and resistance of the junction, respectively. We can express Eq. 5.4 in normalized units by dividing through by the critical current, I_C, giving us

$$\beta_C\frac{d^2\phi}{d\tau^2}+\frac{d\phi}{d\tau}+\sin\left(\phi\right)=i_{dc}+i_{lo}\sin\left(\Omega\tau\right)+\delta i_n\left(\tau\right). \tag{5.5}$$

$\beta_C=\frac{2eI_CR^2}{\hbar}C$ is a normalized parameter of the junction's capacitance, $\tau=\frac{2eI_CR}{\hbar}t$ is normalized time, $i_{dc}=\frac{I_{DC}}{I_C}$ is normalized current, $i_{lo}=\frac{I_{LO}}{I_C}$ is normalized LO current, $\Omega=\frac{\hbar 2\pi f_{LO}}{2eI_CR}$ is the normalized frequency, and $\delta i_n=\frac{\delta I_N}{I_C}$ is the normalized noise source. δi_n is modeled with an average of zero and variance dependent upon the normalized temperature, Γ. The normalized temperature is the ratio of the thermal energy to the Josephson binding energy and is defined as $\Gamma=\frac{2ek_BT}{\hbar I_c}$. The variance of the noise source is then expressed as $\sigma^2=\frac{2\Gamma}{\Delta\tau}$. It is important to note that the noise of the mixer can exceed the thermal noise associated with the bath temperature since room temperature radiation is coupled to the device.

The device was cooled in a helium cryostat to 4 K and the Current-Voltage ($I-V$) characteristics were recorded. We first begin with the static $I-V$ curve where no RF is applied. The HI-JJ exhibited an I_CR_N of about 1.1 mV with a resistance R_N of 11 Ω. From the RCSJ model we obtained a fit to the data, where $\beta_c=0.81$ and $\Gamma=0.002$. The fit to the $I-V$ curve is shown in Fig. 5.4. We then use the obtained junction parameters to begin our fitting to the pumped $I-V$ case.

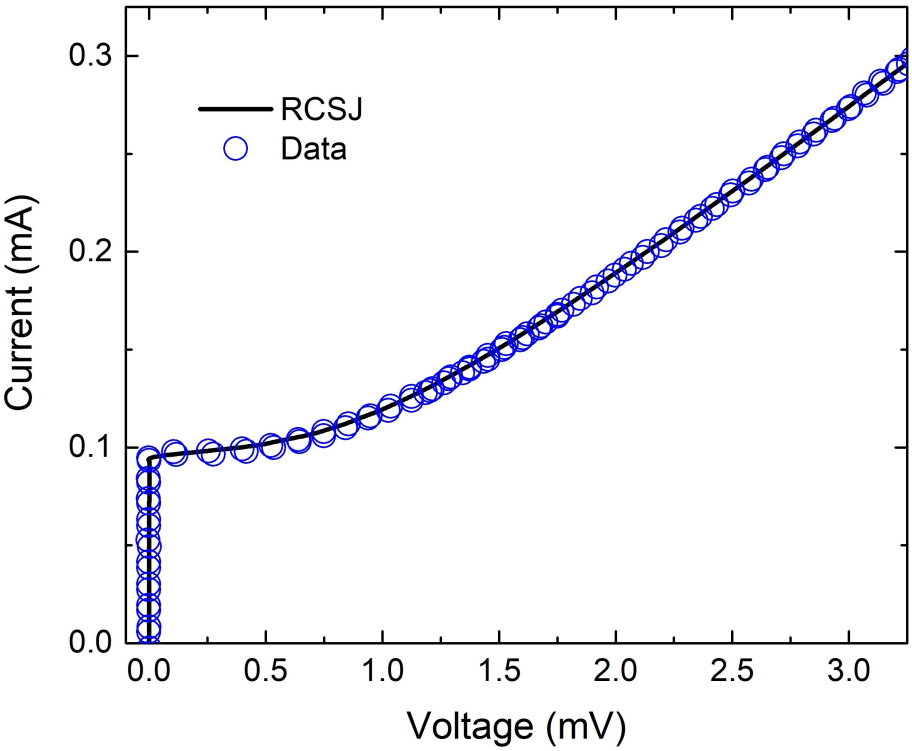

Figure 5.4: Plot of the static I-V data (circles) with the RCSJ fit (solid line). Parameters used for the fit: $\beta_c = 0.81$, and $\Gamma = 0.002$. The RCSJ fit was converted to units in mV and mA by multiplying the normalized current by $I_C = 0.099$ mA and the normalized voltage by $I_C R_N = 1.1$ mV.

Radiation was applied from a 90 GHz Gunn oscillator connected to a tripler, delivering approximately 250 GHz of radiation to the device. Shapiro steps are observed according to the AC Josephson relation: $V = nh\nu/2e$, where n is an integer and ν is the drive frequency [12]. To model the AC Josephson effect we added a time dependent current, $I_{LO} sin(2\pi f_{LO} t)$, to the RCSJ equivalent circuit. We applied varying LO powers to the device and recorded its corresponding I-V and the IF output power as shown in Fig. 5.5. As we increase the LO power we can see suppression of the critical current at the zero-voltage state. The IF power is also effected by the applied LO power and a plot superimposing the various IF output powers are plotted in Fig. 5.6. Ideally, we would like

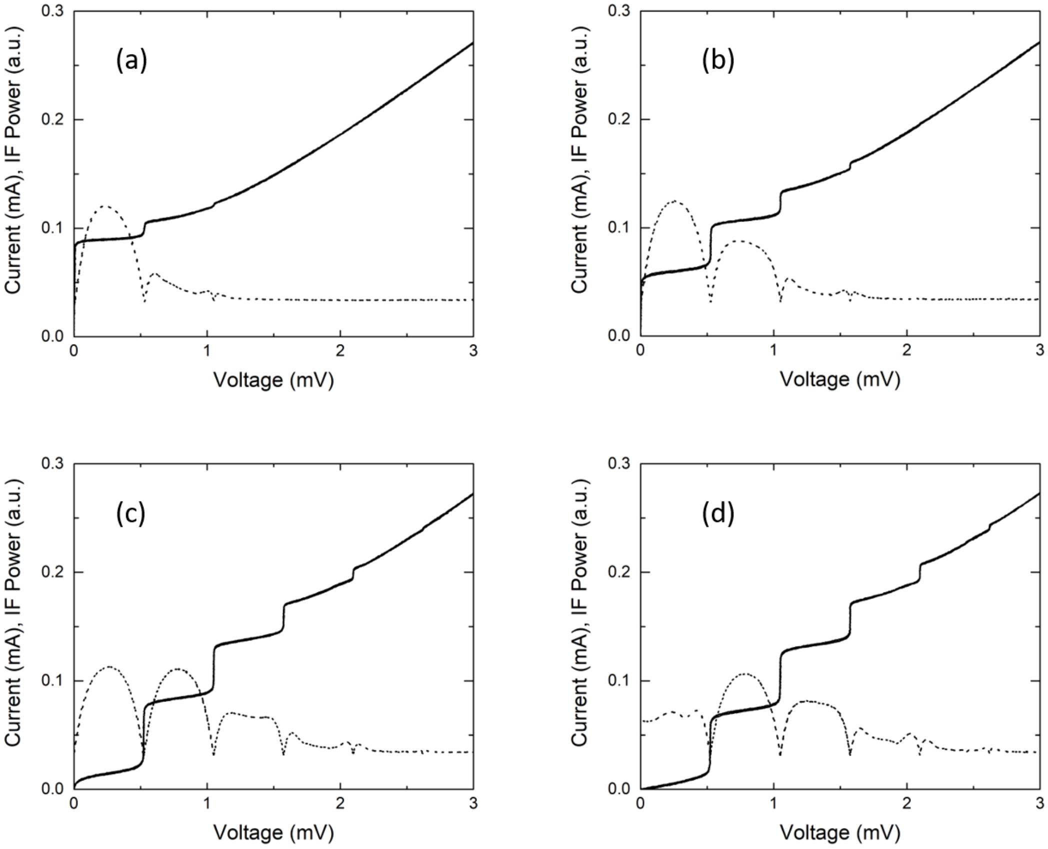

Figure 5.5: Irradiated I-Vs are plotted for varying values of LO power. The corresponding IF power is also plotted as a dotted line.

to operate with the maximum IF power. Previous work has shown that the optimal bias point is halfway between the zeroth and first order Shapiro step. Similarly, from previous work, the optimal pump power occurs when the critical current is reduced to half the critical current in the absence of RF radiation. We use the parameters obtained from the static $I - V$ fit to determine the incident RF power received by the device. With $i_{lo} = 0.79$, we obtained the fit to the pumped case which reveals 3 Shapiro steps shown in Fig. 5.7. In addition to the DC voltage we must solve for the LO voltage. This is achieved through means of a Fourier transform over a minimum of ten LO cycles $\left(10\left(\frac{2\pi}{\Omega_{LO}}\right)\right)$. The LO

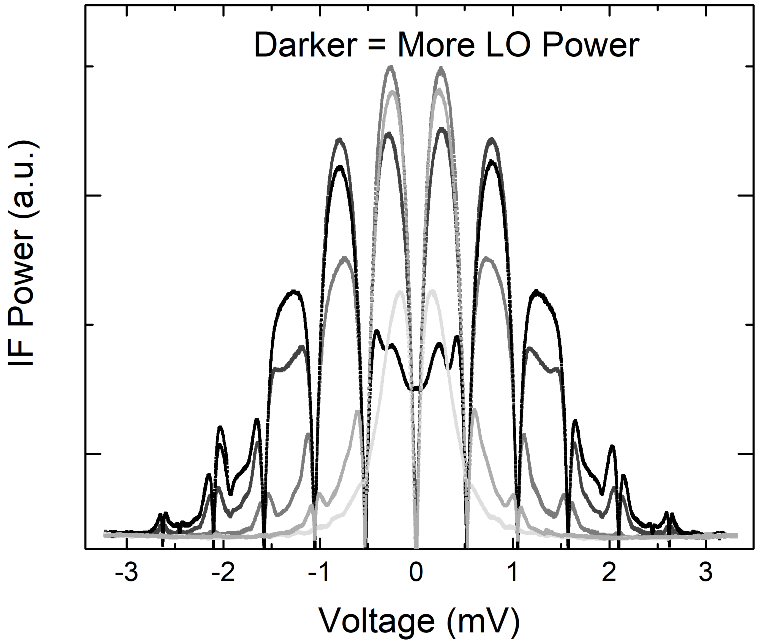

Figure 5.6: Plotting the IF output power of the device for varying LO powers. The darker shade corresponds to a larger LO power used.

voltages are solved for the same parameters used to fit the pumped data and is shown in Fig. 5.8. Once the functions for the DC and LO voltages with dependence on LO power are obtained, we can now solve for the impedance matrix elements and ultimately determine the conversion efficiency of the HI-JJ mixer.

One can obtain the impedance matrix elements from the DC and LO voltage functions and their derivatives. Following general mixer theory the matrix elements of $\tilde{Z}$

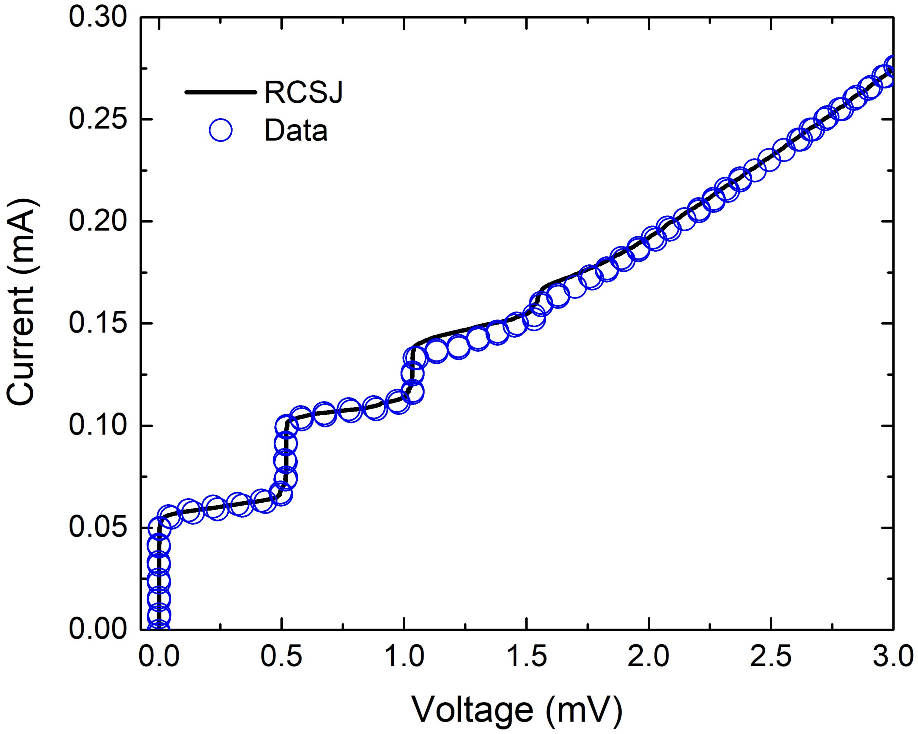

Figure 5.7: Plot of the pumped I-V data (circles) with the RCSJ fit (solid line) at 251 GHz. Parameters used for the fit: $i_{lo} = 0.79$, $\beta_c = 0.81$, $\Omega_{lo} = 0.4676$ and $\Gamma = 0.015$. The RCSJ fit was converted to units in mV and mA by multiplying the normalized current by $I_C = 0.099$ mA and the normalized voltage by $I_C R_N = 1.1$ mV.

are [64, 65]

$$Z_{UU} = \frac{1}{2}\left(\frac{\partial\langle v_{lo}\rangle}{\partial i_{lo}} + \frac{\langle v_{lo}\rangle}{i_{lo}}\right), \qquad Z_{UO} = \frac{\partial\langle v_{lo}\rangle}{\partial i_{dc}},$$

$$Z_{UL} = \frac{1}{2}\left(\frac{\partial\langle v_{lo}\rangle}{\partial i_{lo}} - \frac{\langle v_{lo}\rangle}{i_{lo}}\right), \quad Z_{OU} = \frac{1}{2}\frac{\partial\langle v_{dc}\rangle}{\partial i_{lo}}, \tag{5.6}$$

$$Z_{OO} = \frac{\partial\langle v_{dc}\rangle}{\partial i_{dc}}.$$

In the limit where the intermediate frequency is much smaller than the LO frequency, the

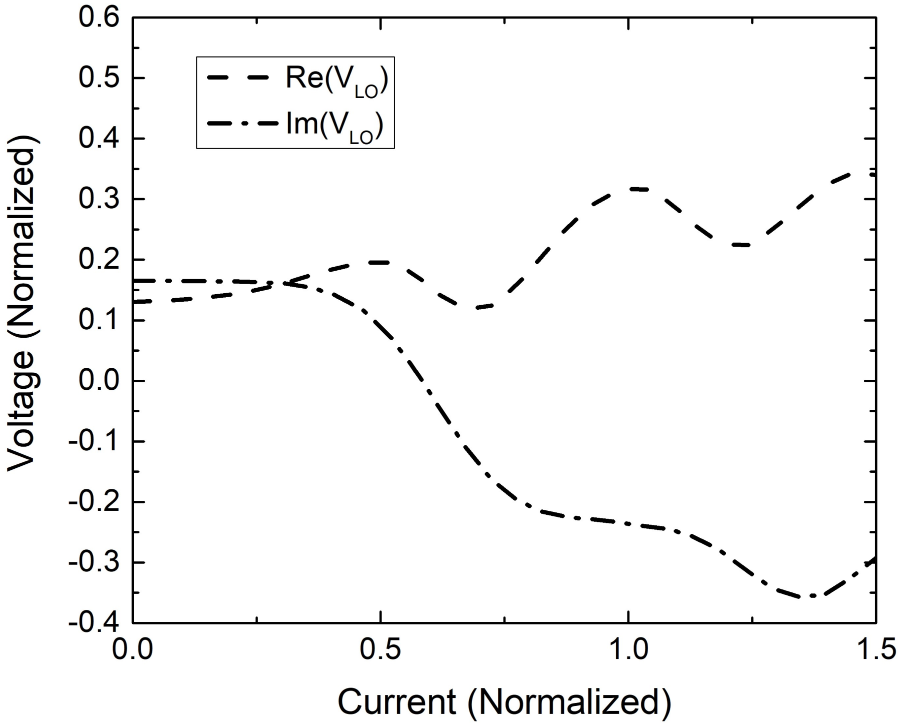

Figure 5.8: Plot of the LO voltage function for the same parameters described in Fig. 5.7. The real component is plotted with dashed lines and the imaginary component is plotted with the dash-dot-dash line. The x-axis is normalized current $\left(\frac{I_{DC}}{I_C}\right)$ and the y-axis is normalized voltage $\left(\frac{V_{DC}}{I_C R_N}\right)$.

conversion matrix, $\tilde{Z}$, is symmetric and the remaining matrix elements are

$$\begin{aligned} Z_{OL} &= Z_{OU}, \\ Z_{LU} &= Z_{UL}^*, \\ Z_{LO} &= Z_{UO}^*, \\ Z_{LL} &= Z_{UU}^*. \end{aligned} \tag{5.7}$$

After obtaining the LO and DC voltage functions for varying LO powers, we solved for the matrix elements at various DC voltage bias as shown in Fig. 5.9. Z_{OU} is related to the down-conversion from the USB to the IF signal, Z_{OO} is the DC dynamic resistance, and

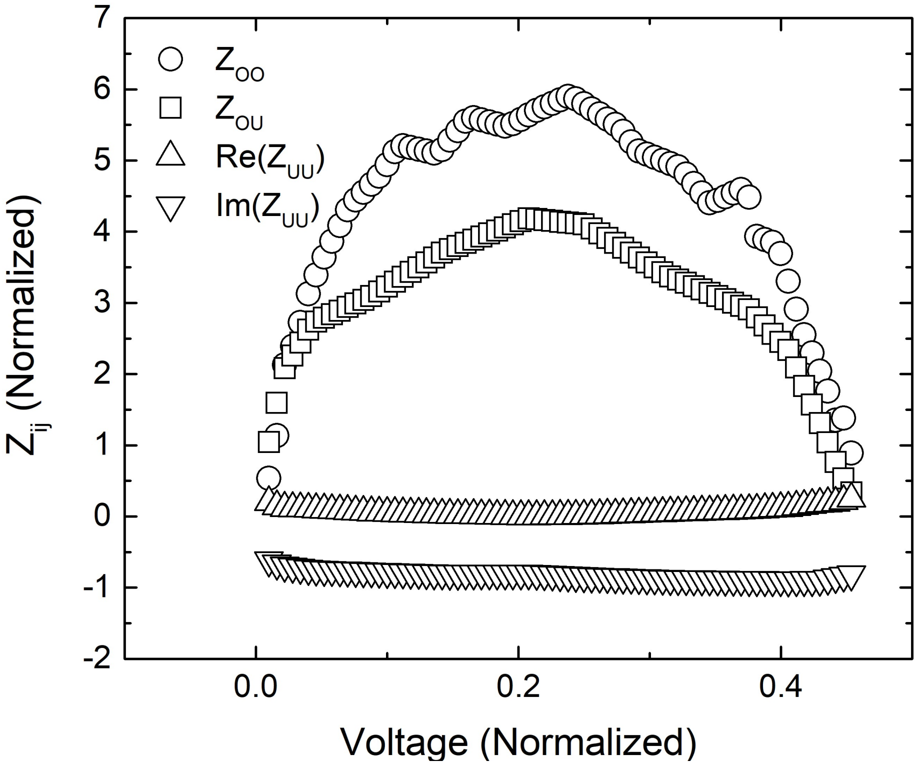

Figure 5.9: Plot of the impedance matrix elements shown in Eq. 5.2, corresponding to the RCSJ fit shown in Fig. 5.7, as a function of voltage. Z_{ij} is normalized to R_N and voltage is normalized by $I_C R_N$. The calculation is focused on the first step of the pumped $I - V$ curve, where optimal DC bias is preferred for mixing operations.

Z_{UU} is the RF impedance. The external part of the circuit must now be included such that we can determine the conversion efficiency. The external impedances connected to the circuit are the upper side-band (Z_U), intermediate frequency (Z_O), and the lower side-band (Z_L). Summing the voltages at all the ports then gives us the following equation:

$$\begin{pmatrix} V_{USB} \\ V_{IF} \\ V_{LSB}^{*} \end{pmatrix} + \begin{pmatrix} Z_U & 0 & 0 \\ 0 & Z_O & 0 \\ 0 & 0 & Z_L \end{pmatrix} \begin{pmatrix} I_{USB} \\ I_{IF} \\ I_{LSB} \end{pmatrix} = \begin{pmatrix} V_{SIG} \\ 0 \\ 0 \end{pmatrix}, \tag{5.8}$$

where V_{SIG} is the incoming signal supplied from the function generator. We approximate Z_U and Z_L as the antenna impedance of 70 Ω for the planar spiral antenna and Z_O is the

50-Ω impedance of the IF line. We can now invert Eq. 5.8 and express the current as:

$$\tilde{I} = \left(\tilde{\tilde{Z}} + \tilde{\tilde{Z}}_{EXT}\right)^{-1} \cdot \tilde{V} = \tilde{\tilde{Y}} \cdot \tilde{V}, \tag{5.9}$$

where $\tilde{\tilde{Y}} = \left(\tilde{\tilde{Z}} + \tilde{\tilde{Z}}_{EXT}\right)^{-1}$ is the admittance matrix. The conversion efficiency of a mixer is defined as the ratio of the delivered IF power to the available RF power, $\eta = P_{\mathrm{IF}}/P_{\mathrm{RF}}$. The available RF power is $P_{RF} = \frac{1}{8}\frac{|V_{SIG}|^2}{Re(Z_U)}$ and the IF power is $P_{IF} = \frac{1}{2}|I_{IF}|^2 Re\left(Z_0\right) = \frac{1}{2}|Y_{OU}V_{SIG}|^2 Re\left(Z_O\right)$. The conversion efficiency is therefore written as

$$\eta = 4\,|Y_{OU}|^2\, Re\left(Z_U\right) Re\left(Z_0\right). \tag{5.10}$$

Solving for the admitaance matrix and substituting into Eq. 5.10 we obtain the conversion efficiency as a function of bias voltage as shown in Fig. 5.10. The maximum conversion efficiency of the HI-JJ mixer at 250 GHz operating at 4 K, at a voltage bias near halfway between the zeroth and first Shapiro step, is approximately $\eta = 0.6$.

While state of the art mixers are comprised of SIS and HEBs, the advancement of technological fabrication techniques has reopened studies into the performance of Josephson Junction mixers [26, 61, 67]. Most attractive are high T_C Josephson mixers since they offer the ability to operate in instruments where passive cooling is the only option, such as space and balloon missions where the cryocooling requirements are important. This work continues the study of Josephson mixers, specifically we investigate the conversion efficiency of a Helium-Ion Josephson Junction mixer operating at 250 GHz. The fabrication technique involved with the creation of these junctions allows for tuning of the junction resistance such that we can better match the antenna impedance to optimize conversion. A fit using the RCSJ model was obtained to the static and pumped $I - V$ characteristics of a HI-JJ with

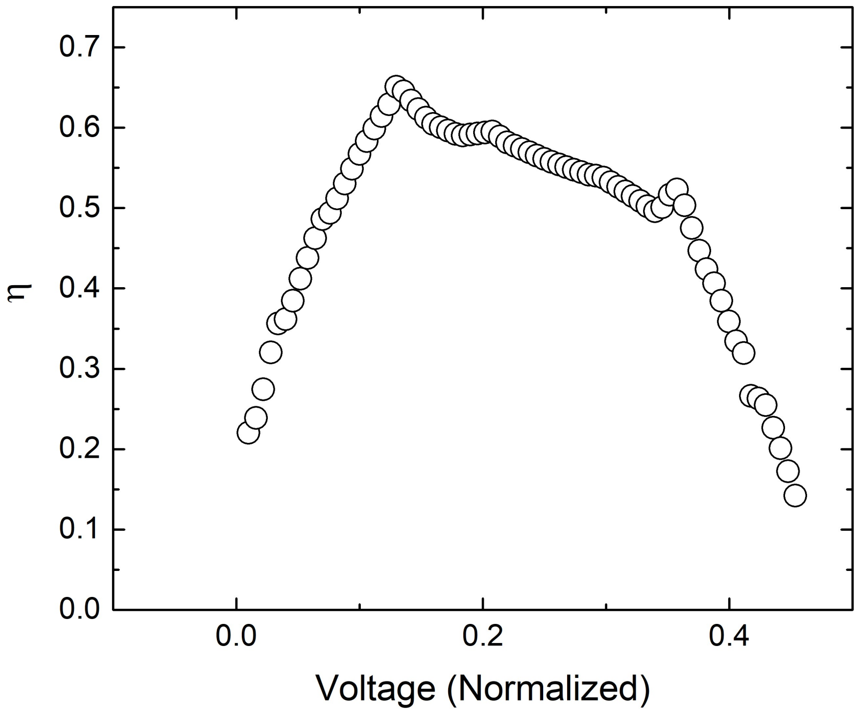

Figure 5.10: Plot of the conversion efficiency as a function of voltage, normalized by $I_C R_N$, focused on the first voltage step of the pumped $I - V$ curve in Fig. 5.7. The normalized external impedance for the upper side-band (Z_U) and intermediate frequency (Z_O) were set to 6.3 and 4.5, respectively.

a critical current of 0.1 mA and a resistance of 11 Ω. From these fits and the three-port model following general mixer theory, we are able to determine the mixer conversion efficiency. From the fitted data we obtained a conversion efficiency of approximately 0.6, corresponding to a conversion gain of -2.2 dB. This is very promising when we compare to the detectors used on the Heterodyne Instrument for the Far Infrared (HIFI) which had conversion gains ranging from -10 dB to -4 dB [68, 69]. This work demonstrates the great potential and flexibility of YBCO junctions directly written with a focused helium ion beam for high frequency applications.

Chapter 6

Conclusions

This dissertation studies the high temperature superconductor YBCO fabricated with Helium Ion Josephson Junctions intended for THz mixing applications. The submillimeter-wave region (300 GHz to 3 THz) of the electromagnetic spectrum is of great interest to the field of astronomy since there exist key spectral lines in this frequency range that provide insight into studying various objects in space such as star formation. Detection of these spectral lines requires high spectral resolution, which heterodyne detectors, also known as mixers, can provide. Current state of the art detectors are Superconductor-Insulator-Superconductor (SIS) mixers and Hot-Electron-Bolometers (HEB). Combinations of these two technologies are required to span the desired submillimeter-wave region. High temperature superconductors that utilize the nonlinearlity associated with the Josephson effect have the potential to span a large frequency range, thus allowing single device operation.

Josephson mixing was first studied and theorized in the 1970's with the use of Nb junctions. These initial studies revealed the importance of impedance matching and acknowledged the higher frequency operation benefits provided by the larger superconducting energy gap associated with high temperature superconductors. Impedance matching within the mixer and circuit components is critical to the device performance. This need for impedance matching has proven difficult for Josephson mixers where the impedance of the junction, typically on the order of a few ohms, is to match the antenna, known to be approximately 75 Ω for a planar spiral. A solution to this mismatch problem can be resolved by utilizing state of the art fabrication tools. Common photolithography techniques typically limit the width of the junction to its minimum feature size. Josephson junctions fabricated with a focused Helium Ion Beam allow for a direct write process with control on the nanometer scale producing nano-wide junctions. Several devices were fabricated with this technique, which resulted in impedance ranging from 5–140 Ω. By varying the dose and width of the junction created one can effectively tune the impedance of the junction to match the antenna.

The current-voltage characteristics of these focused helium ion beam junction devices were recorded. Devices that were well matched to the antenna impedance were selected for AC measurements. Initial measurements consisted of measuring the current voltage characteristics of the devices while a 90 GHz gunn oscillator was irradiated directly into a liquid helium dewar where the device was housed. The current-voltage measurements revealed the extent of the Josephson effect through the expected Shapiro steps. Devices with the best responses at 90 GHz were selected for further measurements at higher frequencies. Various sources allowed inspection of the Josephson Junction's response at 250 GHz, 560 GHz, and 2.5 THz. The Shapiro steps were observed under each of these frequencies, thus demonstrating the Junction's sensitivity and ability to span much of the electromagnetic spectrum.

Selected devices with optimal impedance matching to the antenna were selected and prepped for mixing noise temperature measurements. The convectional Y-factor technique was utilized to determine the mixer noise temperature of these devices. The measured mixing noise temperature at approximately 0.6 THz is competitive when compared to other YBCO Josephson mixers. In addition, we expect improvements by a factor of 5–10 in noise temperature performance by accounting for losses in the system. The conversion efficiency, another figure of merit for mixer performance, was approximated by utilizing fitted data and the three port mixer model. These models also revealed a competitive figure for the focused helium ion beam Josephson mixers. A method to approximate the received RF current was needed in order to predict the conversion efficiency. A previously developed circuit model for RF effects on Josephson junctions was adapted to the novel helium ion beam Josephson junctions which exhibit unique transport properties dependent upon the barrier fabricated. This model proves useful for many other applications outside of mixers where the Josephson junction parameters must be determined.

In the past, Superconductor-Insulator-Superconductor mixers that suppress the Josephson effect proved beneficial in noise performance when compared to the low transition temperate Josepshon Junction mixers due to the associated excess noise. During this time, the potential of a high transition temperature Josephson mixer was apparent, however their complex crystal structures proved difficult for fabrication of devices. With time, many advancements in fabrication tools and techniques improved the feasibility for fabrication of these high transition temperature superconductors. As a result, studies of experimental high T_{C} Josephson mixers began to emerge. This work further studies the potential of Josephson mixers by addressing the known difficulty in impedance matching between the junction and circuit components. The tunable impedance and junction parameters that is afforded by the direct write process involved with the focused helium ion beam proves promising in the possibilities of integrating high T_{C} Josephson mixers in unique space applications where relaxed cryocooling requirements are critical.

Bibliography

[1] D. C. Lis, D. Bockelée-Morvan, R. Güsten, N. Biver, J. Stutzki, Y. Delorme, C. Durán, H. Wiesemeyer, and Y. Okada, "Terrestrial deuterium-to-hydrogen ratio in water in hyperactive comets," *Astronomy & Astrophysics*, vol. 625, p. L5, 2019.

[2] E. Bayet, M. Gerin, T. Phillips, and A. Contursi, "A survey of submillimeter c and co lines in nearby galaxies," *Astronomy & Astrophysics*, vol. 460, no. 2, pp. 467–485, 2006.

[3] J. Zmuidzinas and P. L. Richards, "Superconducting detectors and mixers for millimeter and submillimeter astrophysics," *Proceedings of the IEEE*, vol. 92, no. 10, pp. 1597–1616, 2004.

[4] A. Shurakov, Y. Lobanov, and G. Goltsman, "Superconducting hot-electron bolometer: from the discovery of hot-electron phenomena to practical applications," *Superconductor Science and Technology*, vol. 29, no. 2, p. 023001, 2015.

[5] W. Zhang, P. Khosropanah, J. Gao, E. L. Kollberg, K. Yngvesson, T. Bansal, R. Barends, and T. Klapwijk, "Quantum noise in a terahertz hot electron bolometer mixer," *Applied Physics Letters*, vol. 96, no. 11, p. 111113, 2010.

[6] D. Cunnane, J. Kawamura, M. Wolak, N. Acharya, T. Tan, X. Xi, and B. Karasik, "Characterization of MgB_2 superconducting hot electron bolometers," *IEEE Transactions on Applied Superconductivity*, vol. 25, no. 3, pp. 1–6, 2014.

[7] E. Novoselov and S. Cherednichenko, "Low noise terahertz mgb2 hot-electron bolometer mixers with an 11 ghz bandwidth," *Applied Physics Letters*, vol. 110, no. 3, p. 032601, 2017.

[8] B. Thomas, A. Maestrini, and G. Beaudin, "A low-noise fixed-tuned 300-360-ghz subharmonic mixer using planar schottky diodes," *IEEE Microwave and wireless components letters*, vol. 15, no. 12, pp. 865–867, 2005.

[9] B. Josephson, "Possible new effect in superconducting tunneling," *Phys. Lett.*, vol. 1, pp. 251–253, 1962.

[10] W. Stewart, "Current-voltage characteristics of josephson junctions," *Applied Physics Letters*, vol. 12, no. 8, pp. 277–280, 1968.

[11] D. McCumber, "Effect of ac impedance on dc voltage-current characteristics of superconductor weak-link junctions," *Journal of Applied Physics*, vol. 39, no. 7, pp. 3113–3118, 1968.

[12] S. Shapiro, "Josephson currents in superconducting tunneling: The effect of microwaves and other observations," *Physical Review Letters*, vol. 11, no. 2, p. 80, 1963.

[13] V. Ambegaokar and B. Halperin, "Voltage due to thermal noise in the dc josephson effect," *Physical Review Letters*, vol. 22, no. 25, p. 1364, 1969.

[14] R. Schoelkopf, "Studies of noise in josephson-effect mixers and their potential for submillimeter heterodyne detection." 1996.

[15] K. Likharev and V. Migulin, "Josephson effect millimeter range receivers/review," *Radiotekhnika i Elektronika*, vol. 25, pp. 1121–1142, 1980.

[16] R. J. Schoelkopf, J. Zmuidzinas, T. G. Phillips, H. G. LeDuc, and J. A. Stern, "Measurements of noise in josephson-effect mixers," *IEEE transactions on microwave theory and techniques*, vol. 43, no. 4, pp. 977–983, 1995.

[17] T. Van Duzer and C. W. Turner, "Principles of superconductive devices and circuits," 1981.

[18] J. G. Bednorz and K. A. Müller, "Possible hight c superconductivity in the ba- la- cu- o system," *Zeitschrift für Physik B Condensed Matter*, vol. 64, no. 2, pp. 189–193, 1986.

[19] M.-K. Wu, J. R. Ashburn, C. Torng, P. H. Hor, R. L. Meng, L. Gao, Z. J. Huang, Y. Wang, and a. Chu, "Superconductivity at 93 k in a new mixed-phase y-ba-cu-o compound system at ambient pressure," *Physical review letters*, vol. 58, no. 9, p. 908, 1987.

[20] E. E. Mitchell, K. E. Hannam, J. Lazar, K. E. Leslie, C. J. Lewis, A. Grancea, S. T. Keenan, S. K. H. Lam, and C. P. Foley, "2D SQIF arrays using 20000 YBCO high R_n josephson junctions," *Supercond. Sci. Technol.*, vol. 29, no. 6, p. 06LT01, 2016.

[21] E. R. Pawlowski, J. Kermorvant, D. Crété, Y. Lemaître, B. Marcilhac, C. Ulysse, F. Couëdo, C. Feuillet-Palma, N. Bergeal, and J. Lesueur, "Static and radio frequency magnetic response of high T_C superconducting quantum interference filters made by ion irradiation," *Supercond. Sci. Technol.*, vol. 31, no. 9, p. 095005, 2018.

[22] B. J. Taylor, S. Berggren, M. O'Brien, M. C. de Andrade, and A. L. de Escobar, "HTS YBCO SQUID array transfer function dependence on inductance parameter," in *2017 16th International Superconductive Electronics Conference (ISEC)*. IEEE, 2017, pp. 1–4.

[23] S. Adachi, A. Tsukamoto, Y. Oshikubo, and K. Tanabe, "Fabrication of small biaxial high-T_c gradiometric SQUID," *IEEE Trans. Appl. Supercond.*, vol. 26, no. 3, pp. 1–4, 2016.

[24] B. Müller, M. Karrer, F. Limberger, M. Becker, B. Schröppel, C. J. Burkhardt, R. Kleiner, E. Goldobin, and D. Koelle, “Josephson junctions and SQUIDs created by focused helium-ion-beam irradiation of $YBa_2Cu_3O_7$,” *Phys. Rev. Appl.*, vol. 11, p. 044082, Apr 2019. [Online]. Available: https://link.aps.org/doi/10.1103/PhysRevApplied.11.044082

[25] B. Karasik, W. McGrath, and M. Gaidis, “Analysis of a high-tc hot-electron superconducting mixer for terahertz applications,” *Journal of applied physics*, vol. 81, no. 3, pp. 1581–1589, 1997.

[26] D. Cunnane, J. H. Kawamura, N. Acharya, M. A. Wolak, X. Xi, and B. S. Karasik, “Low-noise thz mgb2 josephson mixer,” *Applied Physics Letters*, vol. 109, no. 11, p. 112602, 2016.

[27] J. Nagamatsu, N. Nakagawa, T. Muranaka, Y. Zenitani, and J. Akimitsu, “Superconductivity at 39 k in magnesium diboride,” *nature*, vol. 410, no. 6824, pp. 63–64, 2001.

[28] R. Fisher, G. Li, J. Lashley, F. Bouquet, N. Phillips, D. Hinks, J. Jorgensen, and G. Crabtree, “Specific heat of mg11b2,” *Physica C: Superconductivity*, vol. 385, no. 1-2, pp. 180–191, 2003.

[29] A. Brinkman, A. A. Golubov, H. Rogalla, O. Dolgov, J. Kortus, Y. Kong, O. Jepsen, and O. Andersen, “Multiband model for tunneling in mgb 2 junctions,” *Physical Review B*, vol. 65, no. 18, p. 180517, 2002.

[30] K. Chen, W. Dai, C. Zhuang, Q. Li, S. Carabello, J. G. Lambert, J. T. Mlack, R. C. Ramos, and X. Xi, “Momentum-dependent multiple gaps in magnesium diboride probed by electron tunnelling spectroscopy,” *Nature communications*, vol. 3, no. 1, pp. 1–5, 2012.

[31] H. J. Choi, D. Roundy, H. Sun, M. L. Cohen, and S. G. Louie, “The origin of the anomalous superconducting properties of mgb 2,” *Nature*, vol. 418, no. 6899, pp. 758–760, 2002.

[32] H. Ekstrom, B. S. Karasik, E. L. Kollberg, and K. S. Yngvesson, “Conversion gain and noise of niobium superconducting hot-electron-mixers,” *IEEE transactions on MIcrowave Theory and Techniques*, vol. 43, no. 4, pp. 938–947, 1995.

[33] E. Gershenzon, M. Gershenzon, G. Gol’tsman, A. Lyul’kin, A. Semenov, and A. Sergeev, “Electron-phonon interaction in ultrathin nb films,” *Sov. Phys. JETP*, vol. 70, no. 3, pp. 505–511, 1990.

[34] F. Boussaha, J. Kawamura, J. Stern, and C. Jung-Kubiak, “2.7 thz balanced waveguide heb mixer,” *IEEE Transactions on Terahertz Science and Technology*, vol. 4, no. 5, pp. 545–551, 2014.

[35] X. Xi, A. Pogrebnyakov, S. Xu, K. Chen, Y. Cui, E. Maertz, C. Zhuang, Q. Li, D. Lamborn, J. M. Redwing *et al.*, “Mgb2 thin films by hybrid physical–chemical vapor deposition,” *Physica C: Superconductivity*, vol. 456, no. 1-2, pp. 22–37, 2007.

[36] X. Gao, J. Du, T. Zhang, and Y. J. Guo, “Noise and conversion performance of a high-t c superconducting josephson junction mixer at 0.6 thz,” *Applied Physics Letters*, vol. 111, no. 19, p. 192603, 2017.

[37] J. S. Tsai, I. Takeuchi, J. Fujita, S. Miura, T. Terashima, Y. Bando, K. Iijima, and K. Yamamoto, “Tunneling study of clean and oriented y-ba-cu-o and bi-sr-ca-cu-o surfaces,” *Physica C: Superconductivity*, vol. 157, no. 3, pp. 537–550, 1989.

[38] K. Hirata, K. Yamamoto, K. Iijima, J. Takada, T. Terashima, Y. Bando, and H. Mazaki, “Tunneling measurements on superconductor/insulator/superconductor junctions using single-crystal yba2cu3o7- x thin films,” *Applied physics letters*, vol. 56, no. 7, pp. 683–685, 1990.

[39] H. Yi, D. Winkler, and T. Claeson, “Tunneling through grain boundaries of yba2cu3o7 step-edge junctions,” *Applied physics letters*, vol. 68, no. 18, pp. 2562–2564, 1996.

[40] S. A. Cybart, E. Y. Cho, T. J. Wong, B. H. Wehlin, M. K. Ma, C. Huynh, and R. C. Dynes, “Nano josephson superconducting tunnel junctions in $\mathrm{YBa_2Cu_3O_{7-\delta}}$ directly patterned with a focused helium ion beam,” *Nat. Nanotechnol.*, vol. 10, no. 7, p. 598, 2015.

[41] J. Valles Jr, A. White, K. Short, R. Dynes, J. Garno, A. Levi, M. Anzlowar, and K. Baldwin, “Ion-beam-induced metal-insulator transition in y ba 2 cu 3 o 7- δ: A mobility edge,” *Physical Review B*, vol. 39, no. 16, p. 11599, 1989.

[42] S. A. Cybart, Ke Chen, and R. C. Dynes, “Planar $\mathrm{YBa_2Cu_3O_7}$ ion damage josephson junctions and arrays,” *IEEE Trans. Appl. Supercond.*, vol. 15, no. 2, pp. 241–244, June 2005.

[43] N. Bergeal, J. Lesueur, M. Sirena, G. Faini, M. Aprili, J. Contour, and B. 1 Leridon, “Using ion irradiation to make high-T_C josephson junctions,” *J. Appl. Phys.*, vol. 102, no. 8, p. 083903, 2007.

[44] S. A. Cybart, S. M. Wu, S. M. Anton, I. Siddiqi, J. Clarke, and R. C. Dynes, “Series array of incommensurate superconducting quantum interference devices from $\mathrm{YBa_2Cu_3O_{7-\delta}}$ damage josephson junctions,” *Appl. Phys. Lett.*, vol. 93, no. 18, p. 182502, 2008. [Online]. Available: https://doi.org/10.1063/1.3013579

[45] E. Y. Cho, Y. W. Zhou, J. Y. Cho, and S. A. Cybart, “Superconducting nano josephson junctions patterned with a focused helium ion beam,” *Applied Physics Letters*, vol. 113, no. 2, p. 022604, 2018.

[46] E. Y. Cho, M. K. Ma, C. Huynh, K. Pratt, D. N. Paulson, V. N. Glyantsev, R. C. Dynes, and S. A. Cybart, “$\mathrm{YBa_2Cu_3O_{7-\delta}}$ superconducting quantum interference devices with metallic to insulating barriers written with a focused helium ion beam,” *Appl. Phys. Lett.*, vol. 106, no. 25, p. 252601, 2015.

[47] E. Y. Cho, H. Li, J. C. Lefebvre, Y. W. Zhou, R. C. Dynes, and S. A. Cybart, “Direct-coupled micro-magnetometer with y-ba-cu-o nano-slit squid fabricated with a

focused helium ion beam," *Appl. Phys. Lett.*, vol. 113, no. 14, Oct 2018. [Online]. Available: http://par.nsf.gov/biblio/10076662

[48] N. Bergeal, X. Grison, J. Lesueur, G. Faini, M. Aprili, and J. Contour, "High-quality planar high-t c josephson junctions," *Applied physics letters*, vol. 87, no. 10, p. 102502, 2005.

[49] S. A. Cybart, P. Roediger, K. Chen, J. Parker, E. Y. Cho, T. J. Wong, and R. C. Dynes, "Temporal stability of y–ba–cu–o nano josephson junctions from ion irradiation," *IEEE Transactions on Applied Superconductivity*, vol. 23, no. 3, pp. 1 100 103–1 100 103, 2012.

[50] Y. Uzawa, M. Kroug, T. Kojima, M. Takeda, M. Candotti, Y. Fujii, K. Kaneko, W. Shan, T. Noguchi, and Z. Wang, "A sensitive alma band 10 sis receiver engineering model," *Superconductor Science and Technology*, vol. 22, no. 11, p. 114002, 2009.

[51] J. Zmuidzinas, H. G. LeDuc, J. A. Stern, and S. R. Cypher, "Two-junction tuning circuits for submillimeter sis mixers," *IEEE Transactions on Microwave Theory and Techniques*, vol. 42, no. 4, pp. 698–706, 1994.

[52] R. Arpaia, M. Arzeo, S. Nawaz, S. Charpentier, F. Lombardi, and T. Bauch, "Ultra low noise yba2cu3o7- δ nano superconducting quantum interference devices implementing nanowires," *Applied Physics Letters*, vol. 104, no. 7, p. 072603, 2014.

[53] S. Nawaz, R. Arpaia, F. Lombardi, and T. Bauch, "Microwave response of superconducting y ba 2 cu 3 o 7- δ nanowire bridges sustaining the critical depairing current: Evidence of josephson-like behavior," *Physical review letters*, vol. 110, no. 16, p. 167004, 2013.

[54] R. Arpaia, S. Nawaz, F. Lombardi, and T. Bauch, "Improved nanopatterning for ybco nanowires approaching the depairing current," *IEEE transactions on applied superconductivity*, vol. 23, no. 3, pp. 1 101 505–1 101 505, 2013.

[55] S. Nawaz, R. Arpaia, T. Bauch, and F. Lombardi, "Approaching the theoretical depairing current in yba2cu3o7- x nanowires," *Physica C: Superconductivity*, vol. 495, pp. 33–38, 2013.

[56] R. Schoelkopf, T. Phillips, and J. Zmuidzinas, "A 100 ghz josephson mixer using resistively-shunted nb tunnel junctions," *IEEE transactions on applied superconductivity*, vol. 3, no. 1, pp. 2250–2253, 1993.

[57] A. T. Cortez, E. Y. Cho, H. Li, D. Cunnane, B. Karasik, and S. A. Cybart, "Tuning y–ba–cu–o focused helium ion beam josephson junctions for use as thz mixers," *IEEE Transactions on Applied Superconductivity*, vol. 29, no. 5, pp. 1–5, 2019.

[58] G. Blonder, M. Tinkham, and T. Klapwijk, "Transition from metallic to tunneling regimes in superconducting microconstrictions: Excess current, charge imbalance, and supercurrent conversion," *Physical Review B*, vol. 25, no. 7, p. 4515, 1982.

[59] R. L. Kautz, "Shapiro steps in large-area metallic-barrier josephson junctions," *Journal of applied physics*, vol. 78, no. 9, pp. 5811–5819, 1995.

[60] J. Clarke, “Finite-voltage behavior of lead-copper-lead junctions,” *Physical Review B*, vol. 4, no. 9, p. 2963, 1971.

[61] M. Malnou, C. Feuillet-Palma, C. Ulysse, G. Faini, P. Febvre, M. Sirena, L. Olanier, J. Lesueur, and N. Bergeal, “High-t c superconducting josephson mixers for terahertz heterodyne detection,” *Journal of Applied Physics*, vol. 116, no. 7, p. 074505, 2014.

[62] J. Du, A. R. Weily, X. Gao, T. Zhang, C. P. Foley, and Y. J. Guo, “Hts step-edge josephson junction terahertz harmonic mixer,” *Superconductor Science and Technology*, vol. 30, no. 2, p. 024002, 2016.

[63] X. Gao, T. Zhang, J. Du, A. R. Weily, Y. J. Guo, and C. P. Foley, “A wideband terahertz high-t c superconducting josephson-junction mixer: electromagnetic design, analysis and characterization,” *Superconductor Science and Technology*, vol. 30, no. 9, p. 095011, 2017.

[64] Y. Taur, “Josephson-junction mixer analysis using frequency-conversion and noise-correlation matrices,” *IEEE Transactions on Electron Devices*, vol. 27, no. 10, pp. 1921–1928, 1980.

[65] H. C. Torrey and C. A. Whitmer, “Crystal rectifiers,” 1948.

[66] R. J. Schoelkopf, “Studies of noise in josephson-effect mixers and their potential for submillimeter heterodyne detection,” Ph.D. dissertation, California Institute of Technology, 1995.

[67] X. Gao, T. Zhang, J. Du, and Y. J. Guo, “340 ghz double-sideband mixer based on antenna-coupled high-temperature superconducting josephson junction,” *IEEE Transactions on Terahertz Science and Technology*, vol. 10, no. 1, pp. 21–31, 2019.

[68] B. D. Jackson, G. de Lange, T. Zijlstra, M. Kroug, T. Klapwijk, and J. Stern, “Niobium titanium nitride-based superconductor-insulator-superconductor mixers for low-noise terahertz receivers,” *Journal of applied physics*, vol. 97, no. 11, p. 113904, 2005.

[69] B. D. Jackson, G. de Lange, T. Zijlstra, M. Kroug, J. W. Kooi, J. A. Stern, and T. M. Klapwijk, “Low-noise 0.8-0.96-and 0.96-1.12-thz superconductor-insulator-superconductor mixers for the herschel space observatory,” *IEEE transactions on microwave theory and techniques*, vol. 54, no. 2, pp. 547–558, 2006.

[70] T. V. Duzer and C. W. Turner, *Principles of Superconductive Devices and Circuits, (Second Ed.).* USA: Prentice Hall PTR, 1998.

[71] A. Barone and G. Paterno, *Physics and Applications of the Josephson Effect.* John Wiley Sons, Ltd, 1982.

[72] S. A. Cybart, E. Cho, T. Wong, B. H. Wehlin, M. K. Ma, C. Huynh, and R. Dynes, “Nano josephson superconducting tunnel junctions in yba 2 cu 3 o 7–δ directly patterned with a focused helium ion beam,” *Nature nanotechnology*, vol. 10, no. 7, p. 598, 2015.

[73] E. Y. Cho, H. Li, J. C. LeFebvre, Y. W. Zhou, R. Dynes, and S. A. Cybart, "Direct-coupled micro-magnetometer with y-ba-cu-o nano-slit squid fabricated with a focused helium ion beam," *Applied physics letters*, vol. 113, no. 16, p. 162602, 2018.

[74] E. Y. Cho, Y. W. Zhou, J. Y. Cho, and S. A. Cybart, "Superconducting nano josephson junctions patterned with a focused helium ion beam," *Applied Physics Letters*, vol. 113, no. 2, p. 022604, 2018.

[75] E. Cho, M. Ma, C. Huynh, K. Pratt, D. Paulson, V. Glyantsev, R. Dynes, and S. A. Cybart, "Yba2cu3o7- δ superconducting quantum interference devices with metallic to insulating barriers written with a focused helium ion beam," *Applied physics letters*, vol. 106, no. 25, p. 252601, 2015.

[76] X. Gao, J. Du, T. Zhang, and Y. J. Guo, "High-t c superconducting fourth-harmonic mixer using a dual-band terahertz on-chip antenna of high coupling efficiency," *IEEE Transactions on Terahertz Science and Technology*, vol. 9, no. 1, pp. 55–62, 2019.

[77] A. Sharafiev, M. Malnou, C. Feuillet-Palma, C. Ulysse, T. Wolf, F. Couëdo, P. Febvre, J. Lesueur, and N. Bergeal, "Hts josephson junctions arrays for high-frequency mixing," *Superconductor Science and Technology*, vol. 31, no. 3, p. 035003, 2018.

[78] P. Rosenthal and E. N. Grossman, "Terahertz shapiro steps in high temperature sns josephson junctions," *IEEE transactions on microwave theory and techniques*, vol. 42, no. 4, pp. 707–714, 1994.

[79] A. Wootten and A. R. Thompson, "The atacama large millimeter/submillimeter array," *Proceedings of the IEEE*, vol. 97, no. 8, pp. 1463–1471, 2009.

[80] G. Pilbratt, J. Riedinger, T. Passvogel, G. Crone, D. Doyle, U. Gageur, A. Heras, C. Jewell, L. Metcalfe, S. Ott *et al.*, "Herschel space observatory-an esa facility for far-infrared and submillimetre astronomy," *Astronomy & Astrophysics*, vol. 518, p. L1, 2010.

[81] K. Akiyama, A. Alberdi, W. Alef, K. Asada, R. Azulay, A.-K. Baczko, D. Ball, M. Baloković, J. Barrett, D. Bintley *et al.*, "First m87 event horizon telescope results. ii. array and instrumentation," *The Astrophysical Journal Letters*, vol. 875, no. 1, p. L2, 2019.

[82] A. Cortez, E. Y. Cho, H. Li, D. Cunnane, B. Karasik, and S. A. Cybart, "High-frequency properties of y-ba-cu-o josephson junctions fabricated with helium ion beam irradiation," in *2019 17th International Superconductive Electronics Conference (ISEC)*. IEEE, 2019.

[83] Y.-T. Wang, R. Semerad, S. J. McCoy, H. Cai, J. LeFebvre, H. Grezdo, E. Y. Cho, H. Li, and S. A. Cybart, "$\mathrm{Yba_2cu_3o_{7-\delta}}$-$\mathrm{ceo_2}$-$\mathrm{yba_2cu_3o_{7-\delta}}$ multilayers grown by reactive co-evaporation on sapphire wafers," *IEEE Transactions on Applied Superconductivity*, vol. 29, no. 5, pp. 1–4, 2019.

[84] P. Hartogh, D. C. Lis, D. Bockelée-Morvan, M. de Val-Borro, N. Biver, M. Küppers, M. Emprechtinger, E. A. Bergin, J. Crovisier, M. Rengel *et al.*, "Ocean-like water in the jupiter-family comet 103p/hartley 2," *Nature*, vol. 478, no. 7368, p. 218, 2011.